Università degli Studi di Firenze

Dipartimento di Chimica

Scuola di Dottorato in Scienze

Dottorato di Ricerca in Scienze Chimiche

XXII Ciclo

CHIM/02-Chimica Fisica

Study of membrane proteins involved in calcium metabolism

Can Phospholamban form ion channels?

PhD. Thesis by

Serena Smeazzetto

Tutor	*Coordinator*
Prof. M. R. Moncelli	Prof. G. Cardini

Contents

List of Figures

List of Tables

Acronyms

ER Endoplasmic reticulum

PLN Phospholamban

SERCA Sarco/endoplasmic calcium ATPase

SR Sarcoplasmic reticulum

BLM Black lipid membranes

PO Phosphatidylcholine

PE Phosphatidylethanolamine

PS Phosphatidylserine

SPHM Phingomyelinospholamban

RF Radio frequency

DC Direct current

MW Microwave

CV Cyclic Voltammetry

AC Alternating current

MHBLM Mixed hybrid-bilayer lipid membrane

SAM Self assembled monolyer

ODT Octadecanethiol

PDOPC Dioleil Phospatidylcholine

TRIS Tris(hydroxymethyl)aminomethane

AFM Atomic force microscope

ChoCl choline cloride

MD Molecular Dynamic

SUV Small unilamellar vesicles

Preface

Life in all its diversity became possible after nature had found the trick with the membrane. Membrane enabled the separation of living entities from the lifeless and the hostile environment under preservation of selective material exchange between the two worlds.[1] Membrane is an extremely complex and elaborate supramolecular structure in which various functional entities (e.g. enzymes, receptors, channels, pigments, etc.) are embedded. Structurally, the lipid bilayer is a very complex system, but it is predominantly composed of various phospholipids. Despite its complexity membrane allows us to explore the interplay between biochemical modulations of the physical properties of biomaterials and the control of biological functions.[1] By reconstitutions of experimental model membranes from a few lipids and membrane proteins, specific function of membrane proteins, isolated from their complex environment, can be studied on a molecular level.
Studying membrane proteins involved in calcium metabolism is of great interest as many physiological precesses and diseases are due to a dysfunction in the regulation of intracellular calcium concentration. During my thesis project I set up and characterized a new biomimetic membrane, namely supported nanoBLMs, in order to study the activity and the selectivity of membrane proteins. Our attention was focused on Phospholamban (PLN), which is a small protein present in the sarcoplasmic reticulum of cardiac myocytes. It regulates the sarco/endoplasmic CaATPase (SERCA) and in this way it is involved in the contractility of cardiac muscles. Various details on the structure of PLN and its activity has puzzled biochemists and biophysicists for many years. In this research project the interest was focused on the controversial issue whether the more stable pentameric form is an ion channel or simply a storage form. In order to understand if PLN pentamer can have ion channel activity, we have performed experiments by using two different biomimetic systems, namely supported nanoBLMs (an experimental model of biological membrane developed recently) and traditional black lipid membranes, BLMs; both systems are characterized by lipid bilayer membranes separating two compartments (cis and trans) containing aqueous solutions and they are mimicking at the best the intra- and the extra- cellular sides of a biological membrane.

Chapter 1

Introduction

1.1 Biological membranes

The basic structure of biomembranes is determined by the lipid bilayer; the functions, however, are mainly performed by membrane proteins, carbohydrates, their complexes, and other constituents such as metallic ions and pigments.[2] A biomembrane is a selective permeability barrier, which allows a controlled interplay and material exchange between compartments performing different functions. The process can be accomplished by either passive, simple or facilitated diffusion or by active transport.[2] At the same time, the biomembrane can carry out essential biochemical functions, such as protein biosynthesis or oxidative phosphorylation. The creation of a barrier opened the possibility for irreversible charge separation (as in the charge transfer chain of mitochondria or photosynthetic membranes) and transient storage of energy in the form of electrochemical potential gradients.[1] Biomembranes enable the formation of intracellular compartments, which was an essential evolutionary step in order to facilitate the control of such a complex machine. Some important consequences and advantages of this organization are:

- The intracellular space is divided into sub-spaces: the lumina of the various organelles and the cytosol;
- Different classes of molecules are distributed among these different subspaces, thus reducing the number of directly interacting molecular species;
- It allows the directed flow of newly synthesized material from the endoplasmic reticulum to the plasma membrane or the extracellular space as well as for the trafficking of nutrition molecules in the opposite direction;
- Different ionic compositions or pH's can be established in the lumina of the various organelles which is essential for the establishment of electrochemical gradients across the membranes, or the control of the activity of specialized proteins (such as the digestive enzymes of lysosomes) and the accumulation of specific proteins within the various subspaces.[1]

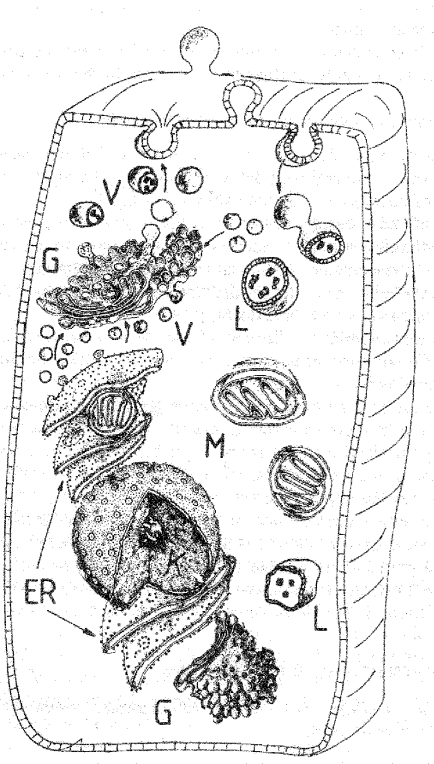

Figure 1.1: *Cartoon of an eucaryotic cell composed of organells with well defined functions. These include: nucleus (K), endoplasmic reticulum (ER), Golgi apparatus (G), mitochondria (M), lysosomes (L) and vesicles (V). Biological membranes divide intracellular space (cytosol), extracellular space and lumina of various organells. Figure from Lipowsky and Sackmann,1995.*[1]

1.1.1 Molecular composition of biological membrane

Biological membranes mainly consist in a phospholipid bilayer in which proteins, peptides, peptaibols and carbohydrates are embedded. The lipid composition and the combination of all these elements exhibit some universal features but also different functions of biological membranes.

Lipid

Only a few classes out of the enormous variety of possible lipids are used by nature to build up animal cell membranes. These may be further divided into a subgroup playing a predominantly structural role and another subgroup with mainly a functional role. Cholesterol, the four major classes of phospholipids (phosphatidylcoline [PC], phosphatidylethanolamine [PE], phosphatidylserine [PS] and sphingomyelin [SPHM]) and cerebrosides belong to the first subgroup. Phosphatidylinositol as precursor of the 2^{nd} messengers belongs to the lipids with a functional role. The membranes of animal cells also contain a substantial amount of neutral lipids such as diacylglycerols and triacylglycerols in addition to fatty acids and lyso-phospholipids.[1]
From the chemical point of view phospholipids are amphipathic and characterized

by three structural features: the size and the electrical property of the head groups which may be charged, zwitterionic or neutral; the number of carbon atoms and double bonds and the structural difference between the two acyl chains of each lipid. Cholesterol, one of the most important steroids, is a principal component of animal cell plasma membranes, and much smaller ammounts are found in the membranes of intracellular organelles. At a membrane level, cholesterol with its hydrocarbon ring structure plays a distinct role in determining membrane fluidity.[2] One of the important effects of cholesterol seems to be on the fluidity of the membrane; it increases the packing density of the phospholipids.[2]

Carbohydrates

Carbohydrates exist in biomembranes as complexes of lipids and proteins, known as glycolipids and glycoproteins, in which sugars are linked to lipid and proteins, respectively. Glycolipids and glycoproteins are interface-active in that they serve as receptor sites for the attachment of other physiological and non-physiological molecules.[2] Since glycolipids show a strong asymmetry in their distribution in the biomembrane, it is presumed that they mediate distinct functions on the cell surface, such as: self recognition (e.g. blood group antigens), electrical effects, cell recognition (e.g. receptors for extracellular species), binding to the extracellular matrix and protection of the cell exterior.

Peptides

Peptides are short polymers formed from the linking, in a defined order, of α-amino acids. The link between one amino acid residue and the next is called an amide bond or a peptide bond. The distinction between proteins and peptides is that peptides are short and polypeptides/proteins are long. Conventionally peptides are defined as polymers not longer than 50 amino acids in length. This definition is somewhat arbitrary, since long peptides, such as the amyloid β peptide (39 - 43 amino acids) linked to Alzheimer's disease, can be considered proteins; and small proteins, such as insulin (51 amino acids), can be considered peptides.

Gramicidin

Gramicidin is a heterogeneous mixture of six antibiotic compounds, which are obtained from the soil bacterial species *Bacillus brevis* and called collectively Gramicidin D. Gramicidin D are linear peptides formed by 15 amino acids. It is known that Gramicidin is a pore forming peptide.

The general formula of Gramicidin is:

formyl-L-X-Gly-L-Ala-D-Leu-L-Ala-D-Val-L-Val-D-Val-L-Trp-D-Leu-L-Y-D-Leu-L-Trp-D-Leu-L-Trp-ethanolamine

where X and Y depend upon the gramicidin molecule. The alternating stereochemical configurations (in the form of D and L) of the amino acids is essential to the formation of the β-helix. The chain assembles inside of the hydrophobic interior of the cellular lipid bilayer to form a β-helix. The helix itself is not long

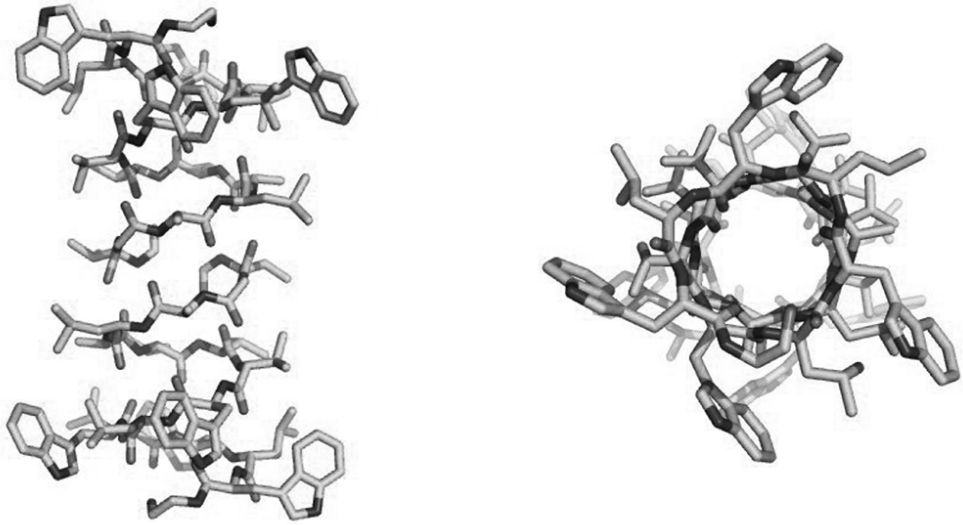

Figure 1.2: *Structure of Gramicidin.*

enough to span the membrane but it dimerizes to form the elongated channel needed to span the whole membrane. Gramicidin D acts as an ion channel with a specific selectivity: NH_4^+, K^+ and Li^+.[3,4]

Peptaibols

The peptaibols are a family of antibiotic peptides isolated from soil fungi that exhibit anti-bacterial and anti-fungal properties. Their length ranges between 5 and 20 residues. The name peptaibol derives from their chemical composition: peptides containing Aib (α-aminoisobutyric acid or α-methyl alanine) residues and ending in a C-terminal alcohol. They also often contain the residue Iva (isovaleric acid or α -ethyl alanine) and many have a number of imino acids, either proline or hydroxyproline. Aib residues tend to promote formation of helical structures due to the steric constraints imposed by the second methyl group on the Cα atom. All peptaibol structures determined to date are highly helical. The imino acids tend to promote formation of bends or kinks in these structures. Peptaibols are amphipathic in nature and this property allows many of them to form voltage-dependent ion channels in lipid bilayer membranes. Leakage of cytoplasmic material can occur through such channels, leading to cell death, and this may be the basis of their antibiotic function. Nowadays over 200 peptaibols have been sequenced.[5]

Trichogin

Trichogin, isolated from the soil fungi *Trichoderma Longibrachiatum*, is one of the shortest members of the family of the peptaibols (11 residues). Trichogin sequence is:

n-Oct-Aib^1-Gly-Leu-Aib^4-Gly-Gly-Leu-Aib^8-Gly-Ile-Lol (where n-Oct is n-octanoyl and Lol is leucinol).

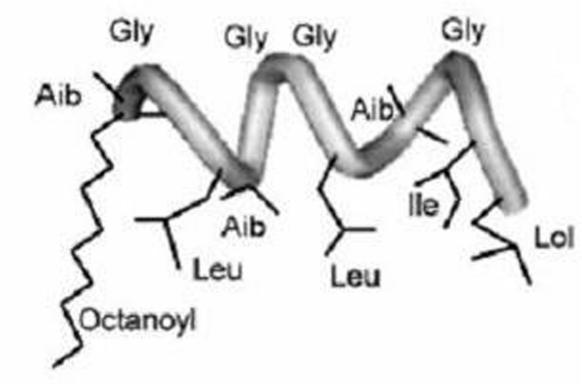

Figure 1.3: *Structure of Trichogin*

This peptide is characterized by 11 residues and a fatty acyl moyety linked to the N-terminal aminoacid (n-octanoil). All peptaibols, whose structures are highly helical (due to the presence of the residue Aib) and amphipatic, exhibit membrane-modifying properties. In particular, the long sequence members, such as alamethicin ($\backsim 30\mathring{A}$), are known to produce voltage-gated channels in planar membranes through which water molecules and ions may easily pass, according to a barrel-stave mechanism.[6] Surprisingly, despite its short main chain, trichogin GA IV exhibits membrane-modifying properties on liposomes comparable to those shown by the long sequence members of the family. Clearly, trichogin is too short (only $16\mathring{A}$) to fully span the membrane and its mechanism of action must be different, at least in part, from that displayed by the long peptaibols.

Membrane proteins

Membrane proteins are proteins that are embedded in (integral), or linked (peripheral) to the membrane of a cell or an organelle.

An integral membrane protein is a protein (or assembly of proteins) that is permanently embedded in the biological membrane. Such proteins can be separated from the biological membranes only using detergents, nonpolar solvents, or sometimes denaturing agents. Peripheral membrane proteins are proteins that adhere only temporarily to the biological membrane. These molecules attach to integral membrane proteins, or penetrate the peripheral regions of the lipid bilayer. In contrast to integral membrane proteins, peripheral membrane proteins tend to collect in the water-soluble component, or fraction, of all the proteins extracted during a protein purification procedure. Membrane proteins can be divided in subgroups characterized by different functions: *structural proteins* are attached to microfilaments in the cytoskeleton which ensures stability of the cell, *cell recognition proteins* allow cells to identify and interact with each other, *membrane enzymes* produce a variety of substances essential for cell function, *membrane receptor proteins* serve as connection between the internal and external environments of the cell and, finally, *transport proteins* that can be carrier proteins or channel proteins.

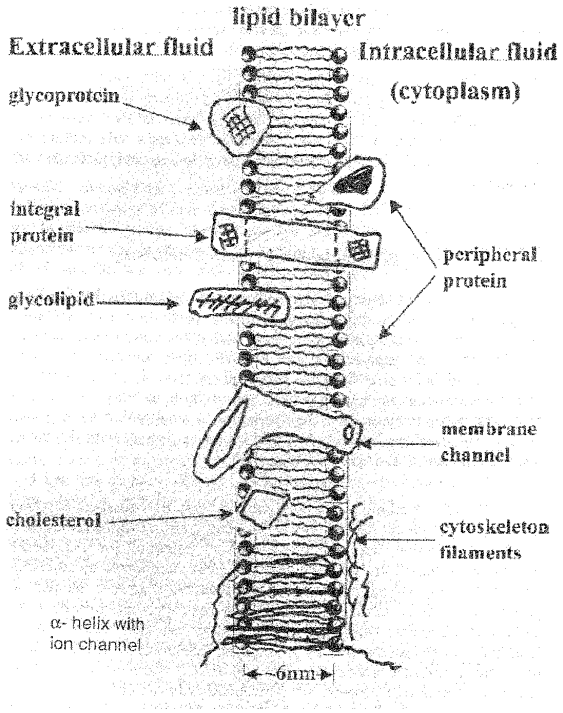

Figure 1.4: *Cartoon of membrane proteins in a lipid bilayer. Figure from Tien and Ottova, 2000*[2]

Phospholamban

Phospholamban (PLN) is a 52 amino acids, integral membrane protein, which is involved in the contractility of cardiac muscle by regulating the intracellular calcium concentration ($Ca^{2+}{}_{cyt}$) of cardiac myocytes. Indeed, relaxation results from the rapid removal of $Ca^{2+}{}_{cyt}$, which is predominantly re-sequestred into the sarcoplasmic (SR) lumen by the sarco/endoplasmatic CaATPase (SERCA), whereas the remaining amount is extruded from the cell by the Na^{+}/Ca^{2+} exchanger and the sarcolemmal CaATPase.[7] PLN modulates $Ca^{2+}{}_{cyt}$ by regulating the SERCA. This membrane protein maintains a low intracellular calcium concentration in the SR by pumping Ca^{2+} into the SR. Activity of SERCA is inhibited by the unphosphorylated PLN whereas phosphorylated PLN releases SERCA inhibition and allows pumping of calcium. PLN monomer ($6KDa$) is in an equilibrium with its pentameric form;[8] the more stable pentamer is a $30KDa$ oligomer in which each monomer is composed of three domains: a helical cytoplasmic domain, a semi-flexible loop and a helical hydrophobic transmembrane domain.[9,10] Various details on the structure of PLN and its activity are still a matter of debate. It is not known whether the interaction with SERCA is due to the monomeric or pentameric form.[11–13] Also structural details of the PLN pentamer are not yet rectified and currently a so called bellflower model[9] and a pinwheel model[14] of the pentamer are discussed in the literature.[9,14–16] Moreover, it is still unknown whether the more stable pentameric form is an ion channel or simply a storage form. During my research project I focused my attention on the function of the PLN pentamer. It is of great interest to understand the

physiological role of phospholamban as it can be a pharmacological target in heart failure. Heart failure is a disease associated with distinct changes in intracellular Ca^{2+} handling. Cardiac relaxation and the rapid removal of cytosolic Ca^{2+} by SERCA are impaired, leading to increased diastolic Ca^{2+} levels. As a result, the load of the cardiac SR is decreased and less Ca^{2+} is available for release in subsequent muscle contractions. Thus a potential therapeutic strategy for heart failure is to enhance the reuptake of Ca^{2+} into the cardiac SR.[17] Indeed it is hoped that strategies targeted to interfere with the phospholamban/SERCA complex may provide a way to solve or at least improve the long-term prognosis of this disease.[7]

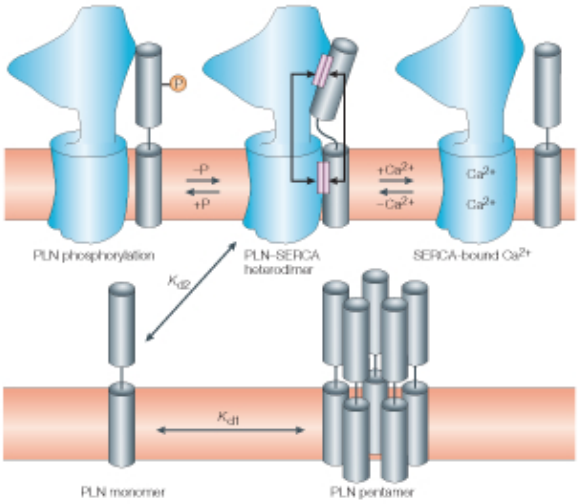

Figure 1.5: *Cartoon of PLN-SERCA interaction. Figure from MacLennan and Kranias, 2003*[18]

1.1.2 Structure and function of biological membrane

All living systems are made of cells, and the lipid bilayer is the essential component. The cell membrane is the primary barrier between the intracellular and extracellular compartments. The lipid bilayer is the universal basis for all biomembrane structure, is made of two layers of lipid molecules and can be seen under electron microscope. Lipid bilayers are only a few nanometers thick ($5 - 10$nm). Biological membrane are characterized by specific chemical and physical properties as described in the following paragraphs.

Semipermeable membrane

Lipid bilayers are semipermeable membrane, meaning that some molecules are allowed to pass freely (diffuse) through the structure, while others can pass only in the presence of specific proteins or protein oligomers.

Self-assembled bilayer

All biomembrane lipids are amphiphilic (amphipatic), meaning that they have hydrophilic polar groups and a hydrophobic hydrocarbon moiety. This dichotomy (or Ying-Yang property) in a single lipid molecule is the primary factor for lipid bilayer formation in aqueous solution. Phospholipids, like other amphiphilic molecules, are subjected to two conflicting forces: the hydrophilic head is attracted to water, while the hydrophobic hydrocarbon moiety avoids water and tend to aggregate with other hydrophobic molecules. This dichotomy is resolved by the formation of a lipid bilayer in aqueous environment. The same forces that drive the amphipatic molecules to self-assemble forming a bilayer confer on that bilayer a self-sealing property. This self-sealing property is important because, if any rip in the lipid bilayer creates a boundary with water, the molecules of the bilayer spontaneously self-assemble to eliminate this boundary since this is energetically unfavourable. If the rip is small, this spontaneous rearrangement leads to the repair of the bilayer, restoring a single continuous layer. If the rip is large, the layer may break up into separate vesicles, forming liposomes.[2]

Bilayer asymmetry

The creation of three different spaces (the lumina, the cytosol and the extracellular fluid) separated by membranes was an essential evolutionary step towards higher forms of life, since it enabled the separation of conflicting biochemical processes such as biosynthesis and degradation. A prerequisite for this division into functional spaces is the vectorial design of the membranes. Essentially all membrane proteins of a given type are oriented in the same way. The specific orientation of integral membrane proteins matches with the asymmetric distribution of the different classes of lipids, even if the real functional role of the lipid asymmetry is not understood yet.[1]

Bilayer fluidity

A fluid lipid bilayer is essential for a cell to live. The aqueous environment inside and outside a cell prevents escaping of membrane lipids from the bilayer. Since membrane is liquid and dynamic it allows moving about, rotating rapidly around their axis and changing places of lipids.[2] Membrane fluidity is important to a cell for many reasons. It enables membrane proteins to diffuse rapidly in the plane of the bilayer and to interact with one another. It allows membranes to fuse with one another and mix their molecules, and it ensures that membrane constituents are distributed evenly between cells when a cell divides. Bilayers undergo a change in state; it is known as phase transition, in which they freeze or melt above or below certain temperatures. At low temperatures, hydrocarbon chains of lipids are tightly packed (gel state), whereas at temperatures above phase transition, the lipid bilayer is in a liquid-crystalline or fluid state. In order to function properly, all membranes must operate at temperatures above phase transition. Phase transition results from temperature-induced changes in packing and mobility of the membrane lipids. The temperature at which lipid phase

transition occurs depends on two factors: length and degree of saturation of fatty acids in the lipids. Lipids with shorter hydrocarbon chains are less rigid and remain fluid at lower temperatures. This is because interaction between shorter chains is weaker than for longer chains. Lipids containing unsaturated fatty acids increase lipid bilayer fluidity since the double bonds introduce kinks, preventing tight packing of fatty acids. On the other hand insertion of cholesterol interferes with interactions between fatty acids, thereby maintaining fluidity at lower temperatures. Rigid rings of cholesterol interact with regions of fatty acid chain adjacent to phospholipid head groups. This interaction decreases the mobility of the outer portions of the fatty acid chains, making this region of the membrane more rigid, even at higher temperatures. An increase in membrane fluidity means that lipid molecules are capable of lateral diffusion in the plane of the membrane. Lateral diffusion is quite rapid and lipids can diffuse from one end of a cell to the other in seconds. However, flip-flop of lipids from one side of the membrane to the other side is normally very slow due to energetics. The difficulty with which flip-flop movement of membrane constituents occurs determines the asymmetric characteristics of the two sides of the membrane. However cholesterol is able to flip-flop from one side of the lipid bilayer to the other side, owing to its small hydrophilic polar group.[2]

Lipid Rafts

Lipid rafts are dynamic plasma membrane microdomains associated with membrane compartmentalization, actin rearrangements, and plasma membrane receptor-mediated signaling events. They are structurally defined as $10 - 200$nm structures, are heterogeneous and highly dynamic biological membrane microdomains enriched in cholesterol and sphingolipids. A wide variety of proteins are known to be targeted to lipid rafts and raft microdomains have thus been associated with a wide range of biological processes, including endocytosis, signal transduction, apoptosis, cell polarization, adhesion, migration, synaptic transmission, and cytoskeleton tethering.[19] Lipid rafts are more ordered and tightly packed than the surrounding bilayer, but float freely in the membrane bilayer.[20]

1.2 Experimental biomimetic models

Considering the complexity of biological membranes and the variables and parameters present, it is necessary to adopt models in order to study the physiological functions. For this reason it is important to use *models*, namely a simply representation of a real system. A model can be experimental or theoretical, based on experiment and observation or based on speculation, respectively. Theoretical models do not have the same impact as experimental models do. In order to study individually single proteins, it is helpful to mimic a biological membrane and embed in it only the protein of interest. In the last fifty years many experimental model membranes have been developed. In the following paragraphs only experimental biomimetic models characterized by aqueous solution on both sides of the membrane will be considered as they mimic at the best the intra- and

extra- cellular sides of a biological membrane. Indeed, the project of this thesis was to characterize a new experimental model of biological membrane, that is nano BLMs.

1.2.1 Bilayer lipid membranes, BLMs

The earliest experimental biomimetic membrane developed was the *bilayer lipid membrane (BLM)* also known as *black lipid membrane*. The first method used to form the BLM is called *painting* method.[21] The term *painting* refers to the process by which these bilayers are made. The term *black membrane* refers to the fact that they are dark in reflected light because the thickness of the membrane is only a few nanometers. To make a BLM, a small aperture is created in a hydrophobic material such as Teflon. The bilayer is formed by spreading a mixture of lipid components dissolved in a hydrocarbon (e.g.decane) across the aperture (1-2 mm diameter) of a septum immersed in an aqueous solution.

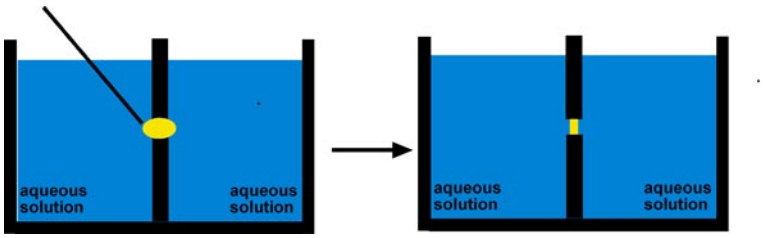

Figure 1.6: *Schematic representation of BLM formation by the painting method.*

Because the aperture (hole), where the BLMs are being formed, is rather small, a low power microscope is used to observe its formation. Initially, the lipid film interposed between two aqueous solutions is relatively thick, which may show intense rainbow colors as thinning occurs. Depending on the lipid solution used, *black* spots suddenly appear in the film after a few seconds to several minutes. These low reflecting black spots grow and come together and eventually fill the entire aperture, except at the bright rim.[2]

Black lipid membranes are well suitable for electrical measurements like resistance (typically $G\Omega$) and capacitance ($2\mu F/cm^2$). Electrical characterization has been particularly important in the study of voltage gated ion channels, which can be inserted into a BLM by dissolving them with a detergent and mixing them into the solution surrounding the BLM. Another way to create BLMs is the so called *folding* method in which the phospholipids in a volatile solvent are spread as monolayers on the surface of the two separated compartments, at the water-air interface. Then the water level is raised in each compartment above the level of the hole to form the bilayer.[22] Folded bilayers are more stable than painted bilayers but are more difficult to obtain. The advantage of this method is that the BLMs formed should be solvent free. Moreover, this method allows asymmetrical membranes to be obtained, with different lipid composition on the two sides.

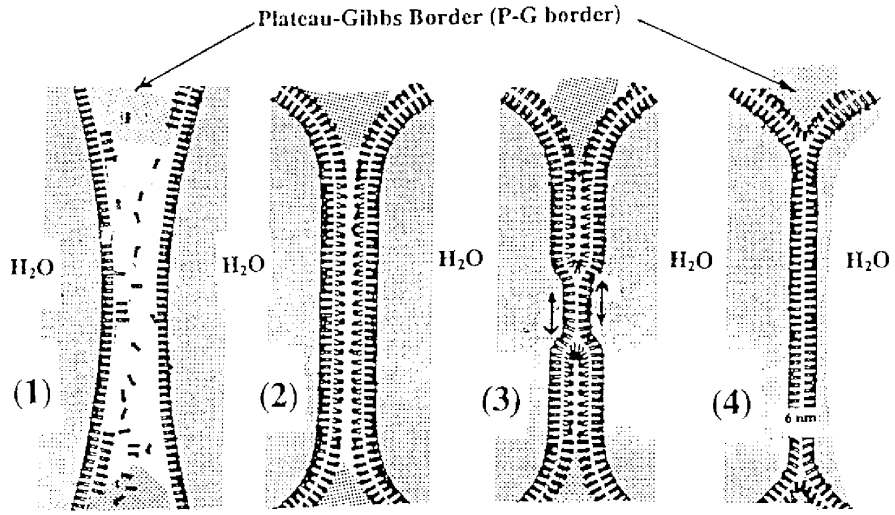

Figure 1.7: *Schematic representation of BLM formation. Figure from Tien and Ottova, 2000*[2]

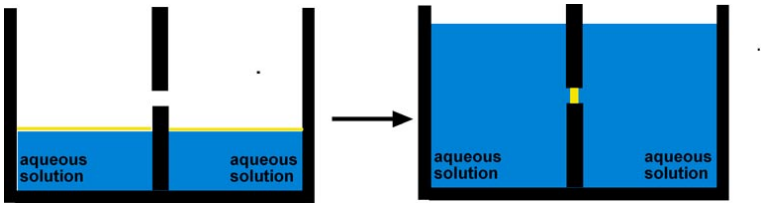

Figure 1.8: *Schematic representation of BLM formation by folding method.*

1.2.2 Pipette method

Bilayers are formed by moving a saline-filled patch-clamp pipette out and into a solution that sustains a lipid monolayer at the air-water interface.

The monolayer can be obtained from lipid solutions in volatile solvents, from dry lipids, or from vesicle suspensions. Formation of membranes is monitored by changes in resistance that take place during movement of the pipettes out, into the air, and back into the solution. As described in Figure 1.9, by moving the pipette out of the solution through a phospholipid monolayer, a phospholipid film is formed at the tip of the pipette. Re-immersion of the pipette into the solution through the monolayer allows the mechanical contact of the hydrophobic tails of both monolayers and the formation of a stable membrane. Upon re-entry of the pipette, a resistance in the giga-ohm range develops instantaneously. Capacitance ranged from 10 to 40 pF and is due to the glass pipette rather than to the membrane itself.[23]

1.2.3 Liposomes

Another widely used model system for biomembranes consists of lipid microvesicles formed by mechanically agitating (or sonicating) a suspension of hydrated amphipatic lipids.[2] Vesicles consist in lipid bilayer rolled up into a spherical

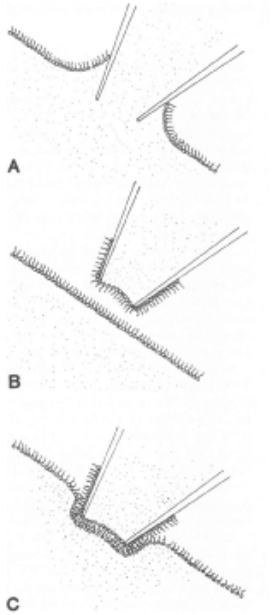

Figure 1.9: *Schematic representation of lipid bilayer formation by the pipette method. Figure from Coronado and Latorre, 1983*[23]

shell, enclosing a small amount of water and separating it from the water outside the vesicle. Vesicles are relatively easy to make, since a sample of dehydrated lipid exposed to water will spontaneously form vesicles. They offer a much larger surface area and more stability than a planar BLM. A major drawback of liposomes is that highly sensitive electrical methods, with a few exceptions, cannot be readily applied to their characterization.

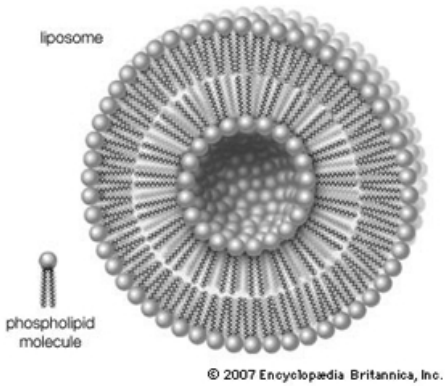

Figure 1.10: *Schematic representation of a liposome and a phospholipid*

1.2.4 Supported nanoBLMs

The conventional BLM system has one major drawback in that it is not very stable, rarely lasting more than 8 h. As a result, many attempts have been made to stabilize this extremely fragile lipid bilayer structure for fundamental studies

and for practical applications.[24] The first report was published in 1978 describing the formation of supported BLMs on polycarbonate filters with improved stability to both chemical and mechanical disturbances.[24] This technique was later resumed and developed by Favero et. al, 2002.[3] They developed Au-supported phospholipid bilayers on a polycarbonate membrane[3].[25] The membranes, separating two aqueous solutions, were formed in microporous filters with pore sizes $1\mu m$ in diameter and densities of 10^5-$10^8 pores/cm^2$. These self-assembled, supported BLMs, not only have overcome the long-term stability problem of the conventional planar lipid bilayers, but also have opened a range of possibilities in manipulating interfacial films as well as in developing practical biosensors.[24]

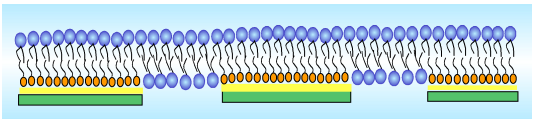

Figure 1.11: *Cartoon of nanoBLMs structure. Polycarbonate membrane in green, gold layer in yellow, octadecanethiol layer in orange and phospholipids in blue. Solution is present on both sides of the membrane.*

Chapter 2

Experimental

2.1 Materials and Instruments

2.1.1 Materials

Ethanol 99.8%, n-hexane 99%, isobutanol 99% were obtained from Fluka (Buchas, Switzerland). Potassium chloride, sodium chloride, sodium perchlorate, hydrocloridric acid fuming 37% and tri-hydroxymethyl-aminomethane (Tris) were purchased from MERCK (Darmstadt, Germany). Dioleoyl-Glycero-Phosphocholine (DOPC) was purchased from Avanti Polar Lipids (Alabaster, AL, USA). Cholesterol was purchased from Aldrich Chemical&Co.(USA). Gold 99,99%, Silver 99,9%, Ottadecanethiol 98% GramD and Choline Chloride 98% were obtained from Sigma-Aldrich (USA). Phospholamban (PLN) and Sarcolipin (SLN) were kindly obtained from Prof. G.Veglia's Group (Minneapolis University, USA). Trichogin was obtained from Prof.Toniolo (Padova University). Polycarbonate membrane filters $1\mu m$ pore diameter ($2 * 10^7 pores/mm^2$, nominal thickness $11\mu m$, nominal weight $1.1 mg/cm^2$) were purchased from SPI-Pore ^{TM} (West Chester, USA). Isopore membrane filters with $0.4\mu m$ pore size and Swinnex plastic cartridges were purchased from Millipore (MA, USA). Cyclopore Track Etched Membranes $1\mu m$ diameter were purchased from Whatman. The porosity of the filter, calculated by SEM image, was 9.5% of the total filter surface (while nominally porosity were in between 4% and 20% and thikness were in between $7\mu m$ and $20\mu m$). Plastic syringes (3ml) were purchased from HSW (Germany). The water was obtained by a double distillation (from reverse osmosis water first and then from potassium permanganate distillation) or by DIRECT-Q system (Millipore, MA, USA).

2.1.2 Instruments

- AGAR AUTOMATIC SPUTTER COATER, $B7341$ (Agar scientific): used to cover Polycarbonate membranes by gold.
- 744 pH-Meter (Metrohm) was used for pH measurements.
- PGSTAT12 Autolab potentiostat/galvanostat (Eco Chemie), with an in-built frequency response analysis FRA2 module: used for electrochemical

measurements (CV Voltammetry, AC Voltammetry and Electrochemical Impedance Spectroscopy). Measurements were controlled by a personal computer, using Autolab GPES and FRA software.

- 712 Conductometer (Metrohm) modified with a resistance of $47K\Omega$ in parallel: used to carry out conductivity measurements.
- Peristaltic pump (ECONO PUMP, BioRad): used to carry out measurements under costant perfusing conditions.

2.2 Techniques

2.2.1 Magnetron sputtering

Sputtering is a technique used to deposit thin films of material onto surface, usually named substrate. The first step is creating a gaseous plasma and then accelerating the ions from this plasma into some source material, named a target. Target is eroded by the arriving ions via energy transfer and is ejected in the form of neutral particles - either individual atoms, cluster of atoms or molecules. As these neutral particles are ejected they will travel along straight line unless they come in contact with other particles or a nearby surface. If a "substrate" such as a polycarbonate membrane is placed in the path of these ejected particles it will be coated by a thin film of the source material. Sometimes described as the "fourth state of matter" (the first three being solid, liquid, gas), a gaseous plasma is actually a "dynamic condition" where neutral gas atoms, ions, electrons and photons exist in a near balanced state simultaneously. An energy source (eg. RF, DC, MW) is required to feed and thus maintain the plasma state while the plasma is losing energy into its surroundings. It is possible to create this dynamic condition by having a known quantity of gas (e.g. Ar) into a pre-pumped vacuum chamber and allowing the chamber pressure to reach a specific level (eg. 0.1 Torr) and introducing an electrode into this low pressure gas environment. The electrode is negatively charged (cathode) and ever present free electrons will immediately be accelerated away from the cathode. These accelerated electrons will approach the outer shell electrons of neutral gas atoms in their path and will drive these electrons off the gas atoms with the formation of positively charged ions (Ar^+). At this point the positively charged ions are accelerated into the cathode, striking the surface and knocking out loose electrode material (diode sputtering) and more free electrons by energy transfer. The additional free electrons feed the formation of ions and the continuation of the plasma. The diode sputtering has proven to be a useful technique in the deposition of thin films when the cathode is covered with source material ("sputtering target"), for instance gold. Diode sputtering however has two major problems: the deposition rate is slow and the electron bombardment of the substrate is extensive and can cause overheating and structural damage. The development of magnetron sputtering deals with both of these issues simultaneously. By using magnets behind the cathode to trap the free electrons in a magnetic field directly above the target surface, these electrons are not free to bombard the substrate to the same extent as with diode

Current (mA)	20
Time (s)	150
Pressure (mbar)	10^{-1}

Table 2.1: *Magnetron sputtering parameters for gold deposition*

sputtering. At the same time the magnetic field affects the path followed by these same electrons when trapped in and the magnetic field enhances their probability of ionizing a neutral gas molecule by several orders of magnitude. This increase in available ions significantly increases the rate at which target material is eroded and subsequently deposited onto the subtrate.

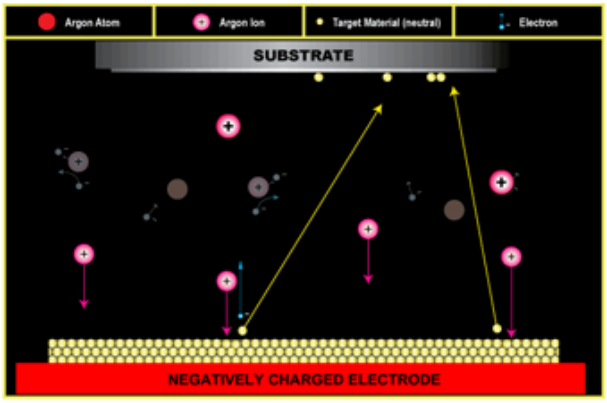

Figure 2.1: *Cartoon of the sputtering process.*

Experimental conditions

During this work the magnetron sputtering technique was used to deposit thin films of gold onto Polycarbonate filters. The parameters used to obtain a good supported membrane are described in Table 2.1.

2.2.2 Cyclic Voltammetry

Cyclic voltammetry or CV is a potentiodynamic electrochemical technique. CV is one of the most popular and versatile techniques for the study of electroactive species. The power of cyclic voltammetry results from its capability to rapidly provide information on redox processes over a wide potential range and it is often the first technique employed in an electrochemical study. In particular, it offers not only a rapid location of redox potentials but also information about the reversible behaviour of the electroactive species. Cyclic voltammetry consists of scanning linearly the potential of a stationary working electrode, which is immersed in an unstirred solution, using a triangular potential waveform (single or multiple cycles can be used), as shown in Figure 2.2.

During the potential sweep, the potentiostat measures the current resulting from the applied potential. The resulting plot of current vs. potential is termed

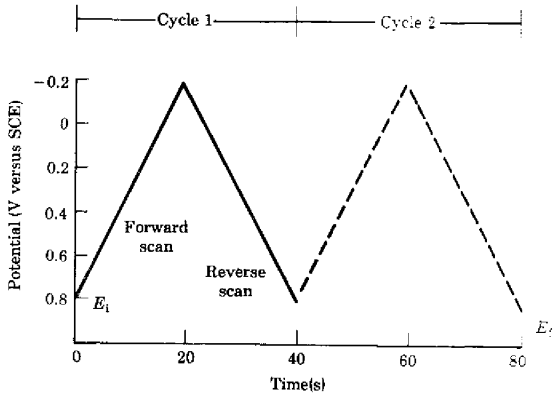

Figure 2.2: *Rapresentative excitation signal for cyclic voltammetry - a triangular potential waveform with switching potentials at* 0.8 *and* −0.2 *V vs. SCE. Figure from Strobel and Heineman, 1989.*[26]

cyclic voltammogram and this plot gives a lot of useful information (Figure 2.3). The principal experimental features of a cyclic voltammogram are:

- the initial potential, E_i; this potential is chosen in a range where the electroactive species is still non active. It depends on the chemical species, the chemical characteristics of the electrode and the nature of the solvent;
- first vertex potential, potential at which the working electrode's potential ramp is inverted;
- the final potential, E_f;
- the scan rate , v_s , the slope of the ramp.

From a cyclic voltammogram we can obtain the following data:

- cathodic peak current, i_{pc};
- anodic peak current, i_{pa};
- cathodic peak potential, E_{pc};
- anodic peak potential, E_{pa}.

These parameters are showed in Figure 2.3. One method for measuring the peak current, i_p is estimated using an extrapolation procedure. The formal reduction potential, $E^{'}$ for a reversible couple is centered between E_{pa} and E_{pc}

$$E^{'} = \frac{E_{pa} + E_{pc}}{2} \tag{2.1}$$

The number of the electrons (n) transferred in the electrode reaction for a reversible couple can be determined from the separation between the peak potentials, ΔE_p which at 25°C is:

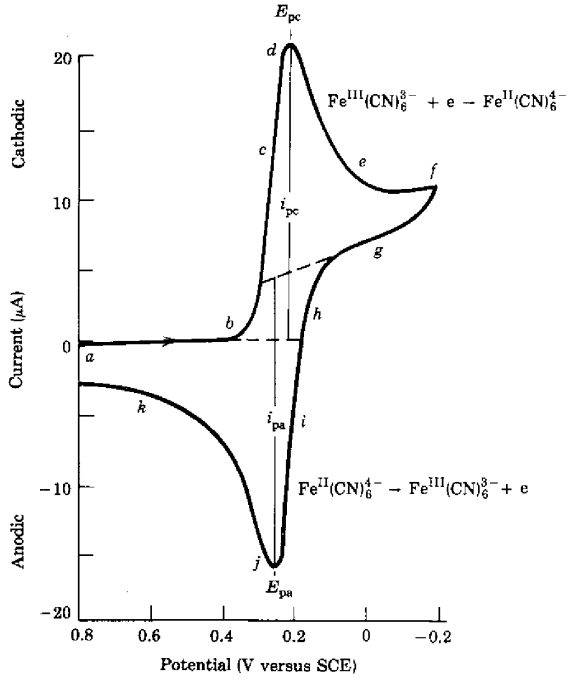

Figure 2.3: *Cyclic voltammogram of* 6 *mM* $K_3Fe(CN)_6$ *in* 1 *M* KNO_3. *Scan initiated at* 0.8 *V versus SCE in negative direction at* 50 $mV\ s^{-1}$. *Platinum electrode,* A=2.54mm^2. *Figure from Strobel and Heineman, 1989.*[26]

$$\Delta E_p = E_{pa} - E_{pc} = \frac{0.059}{n} \tag{2.2}$$

The peak current for a reversible system is described by the Randles-Sevich equation:

$$i_p = (2.69 * 10^5) n^{3/2} A D^{1/2} c^* v_s^{1/2} \tag{2.3}$$

where i_p is the peak current (A), v_s is the scan rate (V sec^{-1}), c^* is the concentration (mol cm^{-3}), n number of the electrons transferred, D diffusion coefficient (cm^2/s^{-1}), A electrode area (cm^2).[26]

Experimental method

During this work CV was used both to clean electrochemically the gold electrodes and to study nanoBLMs. In order to clean the gold electrodes many cycles of CV voltammetry were carried out (see parameters in Table 2.2)

The cyclic voltammogram obtained in our experiments to study nanoBLMs were analyzed to calculate specific resistance. Considering first Ohm's law ($E = iR$) the cyclic voltammogram slope is $1/R$. Specific resistance was obtained dividing the reciprocal of the slope by the area which is supposed to be occupied by nanoBLMs. The parameters used in our experiments are indicated in Table 2.3.

Standby potential (V)	-0.6
Equilibration time (s)	120
Start potential, E_1 (V)	-0.3
First vertex potential, E_2 (V)	1.5
Second vertex potential, E_1 (V)	-0.3
Scan rate (V s $^{-1}$)	0.01

Table 2.2: *Cyclic voltammetry parameters for gold electrode cleaning*

Standby potential (V)	0
Equilibration time (s)	2
Start potential (V)	-0.05
First vertex potential (V)	0.05
Second vertex potential (V)	-0.05
Scan rate (V)	0.01

Table 2.3: *Cyclic voltammetry parameters*

2.2.3 AC Voltammetry

Alternating current (AC) voltammetry is a frequency-domain technique which involves the superimposition of a small amplitude voltage on a linear ramp (Figure 2.4).

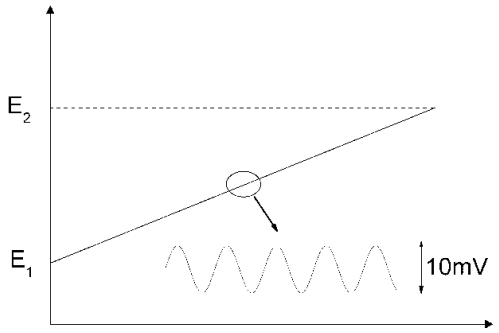

Figure 2.4: *Applied potential in AC Voltammetry*

Usually the alternating potential has a frequency of 50 - 100 Hz and an amplitude of 10 - 20 mV. The AC signal causes a perturbation at the surface of the electrode from which many useful parameters can be obtained. Moreover the non-sinuisoidal (DC) potential is constant during any single cycle of the sinuisoidal wave and can be considered time independent. The results obtained with sinuisoidal wave methods contain mainly capacitive current information. For small amplitudes, the electrochemical interface can be treated as a linear electrical circuit, for which impedance and admittance can be determined. The impedance is related to electrochemical parameters and can be used to obtain information about electrode kinetics, electrosorption, etc. The mathematical analysis can be performed on the results achieved. The current which flows under the su-

perimposition of the sinuisodal potential can be illustrated as composed of two components, one in phase with the excitation voltage ($\phi = 0°$) and one out-of phase angle ($\phi = 90°$). For a signal of magnitude I with phase angle ϕ relative to the excitation, the in-phase component is $I_{ph} = I \sin\phi$ and the out-of phase or quadrature component is $I_q = I \cos\phi$. The total cell current is the vector sum of the in-phase and quadrature components. An electrochemical interface in the absence of faradic processes can be considered as a simple equivalent circuit consisting of a resistance and a capacitance in series Figure 2.5.

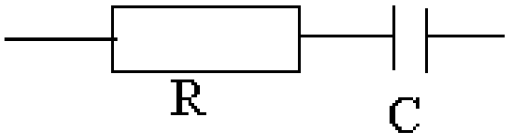

Figure 2.5: *R and C in series*

The total current I which flows trough this circuit can be described by the two sum vectors: I_{ph} and I_q, respectively:

$$I_{ph} = \frac{V}{\omega C\left(R^2 + \frac{1}{\omega^2 C^2}\right)} \tag{2.4}$$

$$I_q = \frac{VR}{R^2 + \frac{1}{\omega^2 C^2}} \tag{2.5}$$

where R is the resistance, C the capacitance, V the alternating potential difference and ω is equal to $2\pi f$ (f=frequency). From the equations 2.4 and 2.5 we can obtain the capacitance value:

$$C = \frac{I_q}{\omega V}\left(1 - \frac{I_{ph}^2}{I_q^2}\right) \tag{2.6}$$

An ideal capacitance has all of its current response at 90° relative to the excitation signal, on the other hand the current response for an ideal resistance is at 0° relative to the excitation signal.

In principle a lipid bilayer can be described by a capacitor if the in-phase component of the electrochemical interface is negligible. That is possible experimentally when the electrolyte concentration is higher than $5 * 10^{-3}$ M, in this situation the equation becomes:

$$C = \frac{I_q}{\omega V} \tag{2.7}$$

Experimental method

The experimental capacitance values were obtained from the quadrature current following a calibration procedure. Calibration was performed by measuring the quadrature current at different capacitance values using a decade capacitor

(type $1412-BC$, General Radio, Concord, MA, USA) and different current range of the potentiostate . The slope of the capacitance vs current plot is the conversion factor that can be used to calculate the capacitance values from the currents recorded in AC voltammetry. In Figure 2.6 an example of this plot is shown. The conversion factor at a sensitivity of $10nF$ is $0.21F/A$.

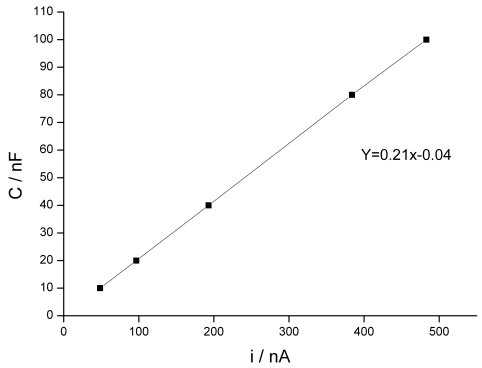

Figure 2.6: *Capacitance vs. current graph.*

Specific capacitance of nanoBLMs is obtained from the capacitance values divided by the area effectively filled by the phospholipid bilayer. The parameters used in our experiments are indicated in Table 2.4.

Standby potential (V)	0
Equilibration time (s)	2
Modulation time (s)	0.21
Interval time (s)	0.61
Frequency (Hz)	75.12
Initial potential (V)	0.05
End potential (V)	-0.05
Step potential (V)	0.01005
Amplitude (V_{rms})	0.01

Table 2.4: *AC voltammetry parameters*

2.2.4 Electrochemical Impedance Spectroscopy

Electrochemical Impedance Spectroscopy (EIS) was developed at the end of 1960's but it started to be extensively studied in early 1980's when the use of computer controlled equipments became available. At the beginning the technique was used in corrosion studies but in recent years EIS has found application in the characterization of interfaces in several fields: coatings, batteries, fuels cells, semiconductors and membranes. The technique has several advantages: it is useful on high resistance materials, can provide time dependent information about

the ongoing process, it is non-destructive and quantitative data are available. The principal disadvantage is the complexity of data analysis for quantification. EIS is a powerful electrochemical tool to characterize intrinsic electrical properties of any material and its interface. The technique is based on the analysis of the impedance in the observed system. This analysis provides quantitative information about the conductance, the dielectric coefficient, the static properties of the interfaces of a system, and its dynamic change due to adsorption or charge-transfer-phenomena.

The technique itself is conceptually rather simple. A low amplitude alternating potential wave is imposed on top of a DC potential. The frequency is varied from as high as 10^5 Hertz to as low as about 10^{-3} Hertz in one experiment in a set number (often between 5 and 10) steps per decade of frequency. Varying frequency from low to high values is also possible. The concept of electrical resistance is well known: it is the ability of a circuit element to resist the flow of electrical current. Ohm's law defines resistance (R) in terms of the ratio between voltage (E) and current (I).

$$\frac{E}{I} = R \tag{2.8}$$

However this relationship can be used only for ideal resistors, which are characterized by the following properties:

- they follow Ohm's law at all current and voltage levels.
- their resistance value is independent of frequency.
- imposed voltage signals and measured AC current through a resistor are in phase with each other.

Usually the real circuit elements exhibit much more complex behaviour, therefore the concept of impedance was introduced. In other words impedance can be defined as a general form of resistance which is not limited by the above simplifying properties. Electrical impedance extends the concept of resistance to AC circuits, describing not only the relative amplitudes of the voltage and current, but also the relative phases. When the circuit is driven with direct current (DC) there is no distinction between impedance and resistance; the latter can be thought of as impedance with zero phase angle. Moreover if a small AC excitation signal is used the system response is pseudo-linear. The excitation signal, expressed as a function of time, has the form

$$E_t = E_0 sin(\omega t) \tag{2.9}$$

where E_t is the potential at time t, E_0 is the amplitude of the signal, and ω is the radial frequency ($\omega = 2\pi f$). In a linear system, the response signal is shifted in phase (ϕ) and has a different amplitude, I_0, as visualized in Figure 2.7.

$$I_t = I_0 sin(\omega t + \phi) \tag{2.10}$$

Considering 2.9 and 2.10 it is possible to write an analogous to Ohm's law:

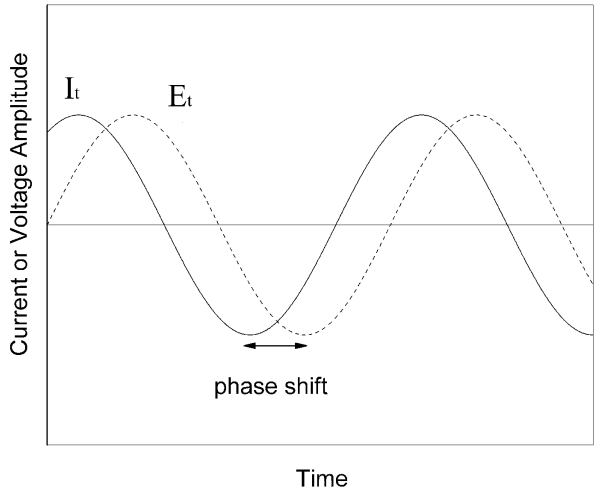

Figure 2.7: *Current and voltage as a function of time. The current response is shifted in time.*

$$Z = \frac{E_t}{I_t} = \frac{E_0 sin(\omega t)}{I_0 sin(\omega t + \phi)} = Z_0 \frac{sin(\omega t)}{sin(\omega t + \phi)} \tag{2.11}$$

where Z is the impedance of the system, moreover it is a complex quantity with a magnitude (Z_0) and a phase shift (ϕ)which depends on the frequency of the signal. Therefore by varying the frequency of the applied signal it is possible to get the impedance of the system as a function of frequency. The impedance can be represented as a complex number in Cartesian co-ordinates:

$$Z(\omega) = Z_r(\omega) + jZ_j(\omega) \tag{2.12}$$

where Z_r is the real part of the impedance and Z_j is the imaginary part and $j = \sqrt{-1}$.

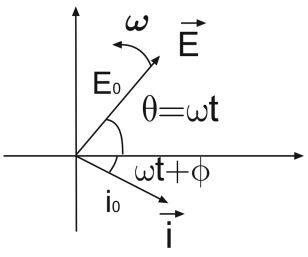

Figure 2.8: *Applied potential and response current vectors in a complex plane.*

The two components can be represented as vectors in a complex plane, (Figure 2.8). The data obtained by EIS are represented typically using Nyquist Plots or Bode Plots.

Nyquist plot

In Nyquist plot (Figure 2.9) the impedance can be represented as a vector of length |Z|. The angle between this vector and the X-axis, commonly called the *phase angle*, is $\phi = argZ$.

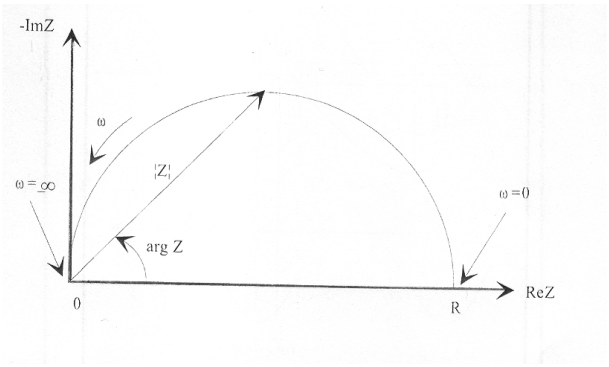

Figure 2.9: *Nyquist plot.*

It can be demonstrated that a simple circuit constituted of a resistance and a capacitance in parallel (Figure 2.10) gives rise to a semicircle whose radius is R/2.

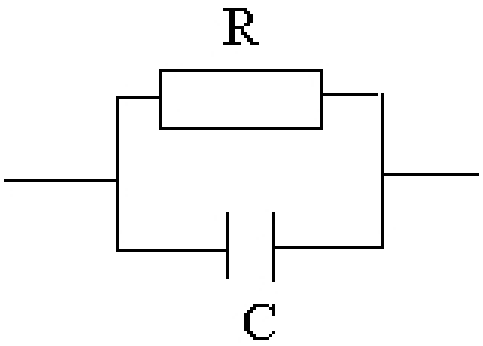

Figure 2.10: *RC mesh.*

Therefore a semicircle is characteristic of a single *time constant* ($\tau = RC$).

Electrochemical Impedance plots often contain several semicircles, sometimes only a portion of a semicircle is seen. The advantage of Nyquist representation is that it gives a quick overview of the data and it allows to make some qualitative interpretations. Plotting data in the Nyquist format the real axis must be equal to the imaginary axis so as not to distort the shape of the curve. The shape of the curve is important in making qualitative interpretations of the data. The disadvantage of the Nyquist representation is that one loses the frequency dimension of the data. One way of overcoming this problem is by labelling the frequencies on the curve.

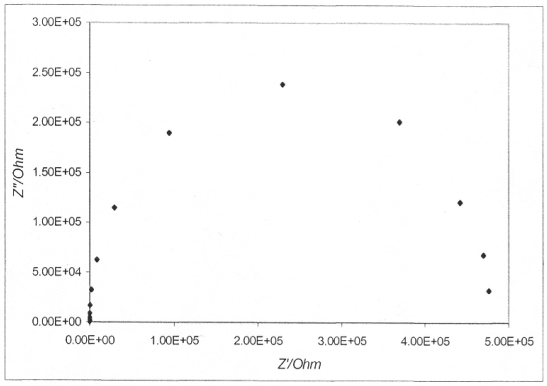

Figure 2.11: *Nyquist plot.*

Bode plot

In the Bode plot the logarithm of the absolute value of the impedance (|Z|) and phase (ϕ) are plotted as a function of the frequency (f) logarithm.

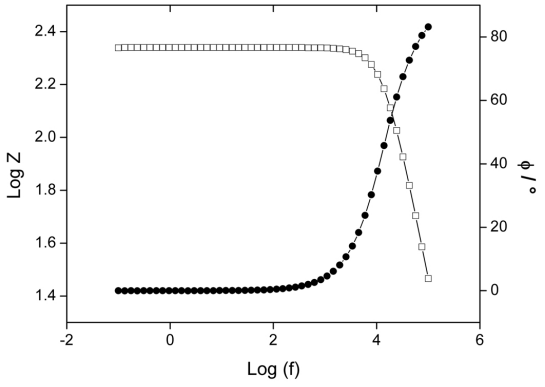

Figure 2.12: *RC Bode plot.*

An advantage of Bode plot is that the impedance behavior at high frequencies is shown with equal weight, along the plot, to that at low frequencies, therefore it is easy to understand how the impedance depends on the frequency. The magnitude of impedance is in a logarithmic scale in order to permit the identification of small impedances in the presence of large ones. EIS data are commonly analyzed by fitting an equivalent electrical circuit model to them. Most of the circuit elements in the model are common electrical elements such as resistors, capacitors and inductors. Table 2.5 represents the most common electrical elements.

Electrical elements, used in the model, should have a basis in the physical electrochemistry of the system. For example, most models contain a resistor that correspond to the cell's solution resistance. Therefore the simplest equivalent circuit for an electrochemical interface is given by Randles circuit (Figure 2.13), which consists in a parallel RC mesh in series to an ohmic resistance representing the electrolyte solution. During this research project, the capacitance and

Component	Current Vs.Voltage	Impedance
Resistor	E= IR	Z = R
Inductor	E = L di/dt	Z = j ω L
Capacitor	I = C dE/dt	Z = $1/j\omega C$

Table 2.5: *Impedance of lectrical components*

resistance values were obtained by fitting the Randles circuit to the experimental data.

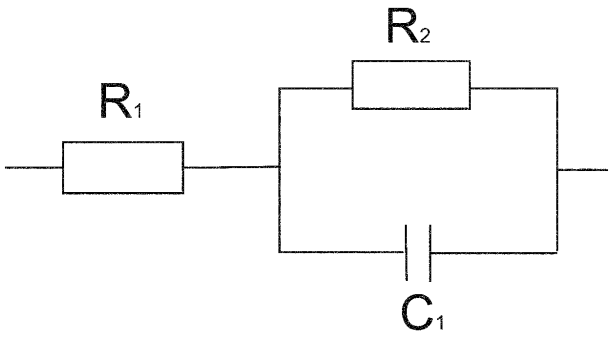

Figure 2.13: *Randles circuit.*

The corresponding Nyquist and Bode plots for this circuit are shown in Figure 2.14.

Experimental method

The obtained data were represented by the Bode plot, which contains all information needed to determine the R and C values of the equivalent circuit. Since in a RC circuit, the value of the time constant (τ, in seconds) is equal to the product of the circuit resistance (in ohms) and the circuit capacitance (in farads), i.e. τ = R$*$C, each element can be identified at different range of frequency. The optimal frequency range of the measurements has to be chosen considering several aspects as:

- for high frequency values the impedance is determined by the ohmic resistance (R_1);

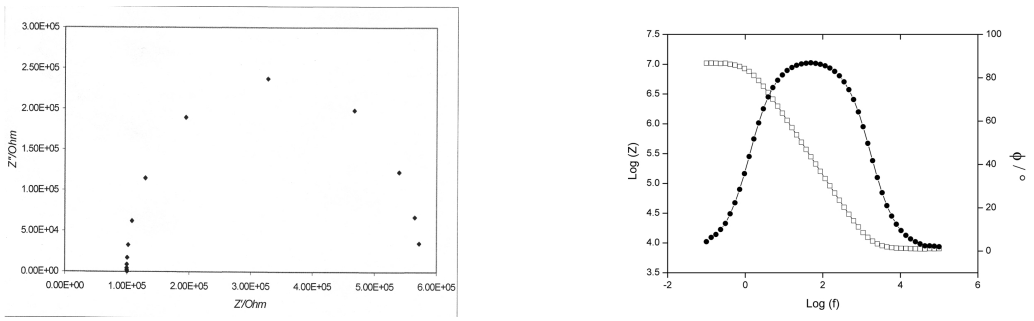

Figure 2.14: *Nyquist and Bode plots of a Randles circuit.*

Standby potential (V)	0
Equilibration time (s)	2
Potential (V)	0
Initial frequency (Hz)	10^6
End frequency (Hz)	0.005
Number of Freq.	31
Step potential (V)	0.01005
Amplitude (V_{rms})	0.014

Table 2.6: *EIS parameters*

- the electrical double layer capacitor shortcuts the Faradic impedance at intermediate frequencies, when the phase angle is 90° (C_1);
- at very low frequencies, when the phase angle is nearly zero, the impedance is determined by the ohmic resistance of the bilayer (R_2).

The parameters used in our experiments are indicated in Table 2.6.

2.2.5 Conductivity measurements

Electrical conduction is a property of ionic solutions. From a macroscopic point of view, ionic conduction of solutions is similar to electron conduction through metals. The conduction in the metals is due to the movements of electrons, in the solutions charges are moving as ions. The conductance of electrolytic solutions depends on the concentration of the ions and also on the nature of the ions present (their charges and mobilities). Since conductance is a function of concentration, it is different for strong and weak electrolytes. If the charge dQ is transferred during time dt, the current obtained from Equation 2.13 is passing through the sample.

$$I = dQ/dt \tag{2.13}$$

Electrolyte solutions obey to Ohm's law just as metallic conductors do. The current I passing through a given body of solution is proportional to the applied potential difference E. The resistance R of a solution in ohms (Ω) is given by:

$$R = E/I \tag{2.14}$$

where the potential difference is expressed in Volts and the current in Amperes. The conductance (G) is defined as the reciprocal of the resistance and it is proportional to the cross-sectional area A and inversely proportional to the length l of a homogeneous body cross section, as shown in Figure 2.15

$$G = 1/R = \kappa A/l \tag{2.15}$$

where κ is the conductivity with units $\Omega^{-1}m^{-1}$ (Ω^{-1} is called Siemens, S):

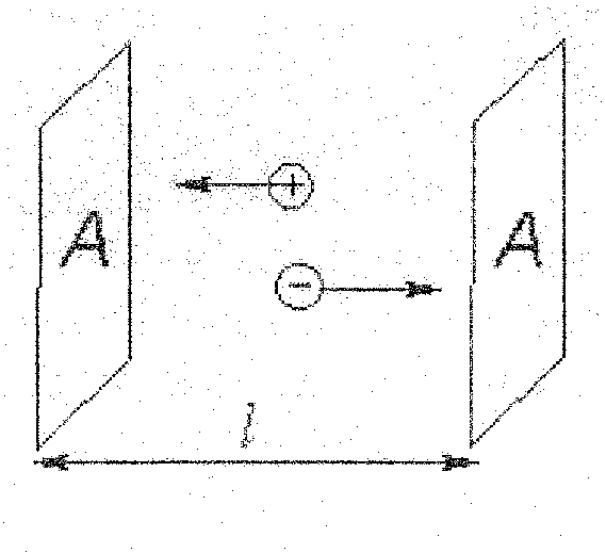

Figure 2.15: *Conductivity representation.*

$$\kappa = l/AR = \Theta/R \tag{2.16}$$

In Equation 2.16, the ratio l/A is a constant for a particular measurement cell, and is hence referred to as the cell constant, Θ, with units m^{-1}. This constant depends on geometrical parameters and any cell should be calibrated by measuring the resistance of the cell filled with a solution of known conductivity, which is invariably KCl (usually $0.01M$). The conductivity, κ, is an intrinsic property of a solution, rather than a property of the conductance cell used. It is important to realize that conductance (and conductivity) values contain more information than simple ion concentrations. That is, the measured conductivity for a solution of 1M HCl will be substantially different than for 1M KCl. This fact arises because protons are much more mobile in solution than potassium ions. Such differences may be quantified by considering the parameter called the mobility (μ) of an ion. The mobility is essentially that part of the conductivity that is independent of concentration. In an ideal case, the mobility of an ion i depends on the charge of the ion (z_i), its solvated radius (R_i), the viscosity of the solvent (η) and the elementary charge (e) according to:

$$u_i = \frac{\mid z_i \mid e}{6\pi\eta R_i} \tag{2.17}$$

The experimental conductivity reflects contributions from all ions present in solution that are mobile and can support the current. Conductivity can be written in terms of the mobilities of all the ions present:

$$\kappa = F^2\Big(\Sigma_i \mu_i z_i^2 c_i\Big) \tag{2.18}$$

where F is the Faraday constant ($96,485C/mol$), and c_i is the concentration of ion i in mol/cm^3. Equation 2.18 shows that conductivity reflects the identity

KCl solutions (mol/dm^3)	$\Lambda(Scm^2mol^{-1}eq^{-1})$
0.001	146.9
0.005	143.5
0.01	141.2
0.02	138.2
0.05	133.3
0.10	128.9

Table 2.7: *Equivalent conductivity values for KCl solutions*

(charge and mobility) of all ions present in solution, as well as their concentrations. From the experimental point of view it is evident that conductivity depends on concentration and measured values for different solutions are not easy to compare directly. For this reason, a quantity called the molar conductivity (Λ_m) is introduced. The molar conductivity (Λ_m) is defined as the solution conductivity (κ) normalized by the total ionic concentration (c):

$$\Lambda_m = \frac{\kappa}{c} \tag{2.19}$$

where c is the molar concentration expressed in units of mol/cm^3. However one can usefully compare the molar conductivities of two electrolytic solutions only if the charges borne by the ions in the two solutions are the same. It means, for instance, that the Λ_m of a $0.1M$ KCl solution is different from the Λ_m of a $0.1M$ $CaCl_2$ solution. We can compare, in principle, the conductivity of the two solutions only if we introduce the concept of equivalent conductivity Λ_{eq}:

$$\Lambda_{eq} = \frac{\kappa}{cz+ \mid z- \mid} = \frac{\Lambda_m}{z+ \mid z- \mid} \tag{2.20}$$

But experimentally the equivalent conductivity varies significantly with the concentration of ions as reported in Table 2.7.

For comparison of conductivities of different compounds, the most useful quantity to consider is the limiting equivalent conductivity, Λ^0. This parameter represents the equivalent conductivity for a compound that would hypothetically be measured in the limit of infinite dilution. In practice, such values are obtained by fitting experimental data to an equation known as Kohlrausch's law :

$$\Lambda_{eq} = \Lambda^{\circ}_{eq} - \kappa\sqrt{c} \tag{2.21}$$

The coefficient κ depends primarily on the type of the electrolyte (e.g., 1:1, 2:1, etc.), rather than its specific chemical identity .

Kohlrausch's extremely careful measurements of the conductance of electrolytic solutions can be considered to have played a leading role in the initiation of the physical chemistry of ionic solutions. Several experimental values of Λ^0 have been carefully determined for many salts as a function of concentration in very dilute solutions. Λ^0 is the intercept values of the resulting plots obtained. In examining such data, it was discovered that Λ_0 for any electrolyte can be expressed as the sum of independent contributions from the constituent cations and

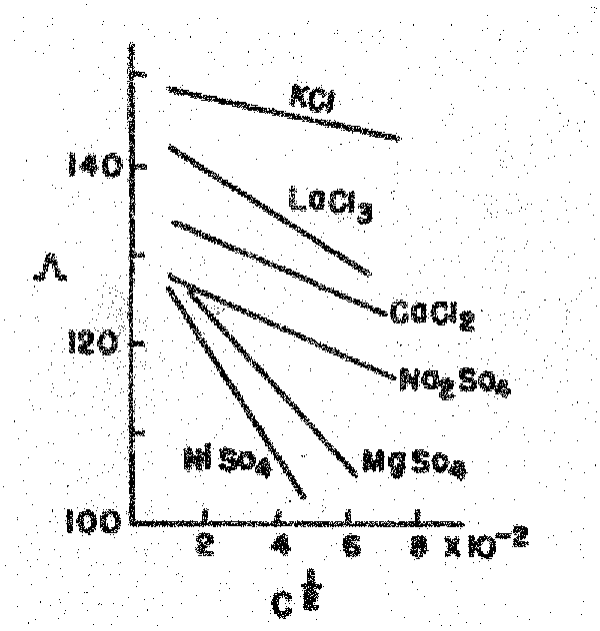

Figure 2.16: *The experimental basis for Kohlrausch's law:* Λ *versus* $c^{1/2}$ *plots are straight lines.*

anions present. This fact is now known as Kohlrausch's Law of the Independent Migration of Ions:

$$\Lambda = \nu_+ \lambda_+^0 + \nu_- \lambda_-^0 \tag{2.22}$$

ν_+ and ν_- represent stoichiometric coefficients for the cation and anion in the electrolyte, respectively.

Experimental method

The conductivity of a solution is highly temperature dependent, therefore it is important to either use a temperature controlled instrument, or calibrate the

Ion	(Λ^0)	Ion	(Λ^0)
H^+	349.8	OH^-	198.6
Na^+	50.1	F^-	55.4
Li^+	38.7	Cl^-	76.3
K^+	73.5	ClO_4^-	67.3
Ca^{2+}	59.5	NO_3^-	71.5

Table 2.8: *Limiting molar conductivity,* Λ^0 *of some ions at* $25°C$

instrument at the same temperature as the solution that you need to measure. Unlike metals, the conductivity of common electrolytes typically increases with increasing temperature. A temperature coefficient (Equation 2.23) is assumed for all ions except H^+ ($0.0139°C^{-1}$) and OH^- ($0.018°C^{-1}$)

$$\alpha = \frac{1}{\lambda_i^0}(\frac{d\lambda_i^0}{dT}) \cong 0.02°C^{-1} \tag{2.23}$$

During this thesis conductivity measurements were carried out by 712 Conductometer (Metrohm). The instrument can be connected to the computer allowing to acquire data continuously. The 712 Conductometer automatically changes the potential difference applied to the cell in response to resistance measured . This technical feature damaged all the obtained bilayers, therefore the instrument was modified by adding a resistance of $47K\Omega$ in parallel. The modified conductometer permits to keep costant the potential difference applied to the cell at $0.5VRMS$. The frequency was set at a fixed value of $2.4KHz$, temperature was settled at 25 $°C$ during the experiments.

2.3 Methods

2.3.1 ODT-SAM formation

A self-assembled monolayer (SAM) of octadecanethiol (ODT) was obtained by spreading $3mM$ ethanolic solution of ODT on the gold layer. Subsequently the ethanol was allowed to evaporate totally and the membrane was rinsed by a series of washing steps in ethanol, water and ethanol to eliminate ODT in excess; at the end it was totally dried. On the top of the gold-polycarbonate membrane, an octadecanethiol self assembled monolayer (SAM-ODT) was formed.

2.3.2 NanoBLMs formation

The working cell was assembled by setting the polycarbonate membrane between the two Teflon blocks and leaving exposed a circular surface of $19.6mm^2$. When the bi-cell was assembled, the DOPC-Cholesterol solution (3:1) in a 1:10 isobutanol:n-esane solvent, was spread on the SAM-ODT surface and $10mM$ TRIS buffer pH=7,5 was continuosly perfused in both the two teflon blocks using a peristaltic pump at $0.1ml/min$. In this way the phospholipid bilayer was formed generating a mixed hybrid-bilayer lipid membrane (MHBLM) on the membrane support. Lipid bilayers were formed on each pore of the polycarbonate membrane as described in Favero et al. 2002 and Favero et al. 2005.[3,25] Previous experiments demonstrated that both gold and octadecanethiol do not occlude the polycarbonate membrane pores,[3] and allow phospholipid bilayer formation in correspondence of the pores (nanoBLMs) as shown in Figure 1.11.

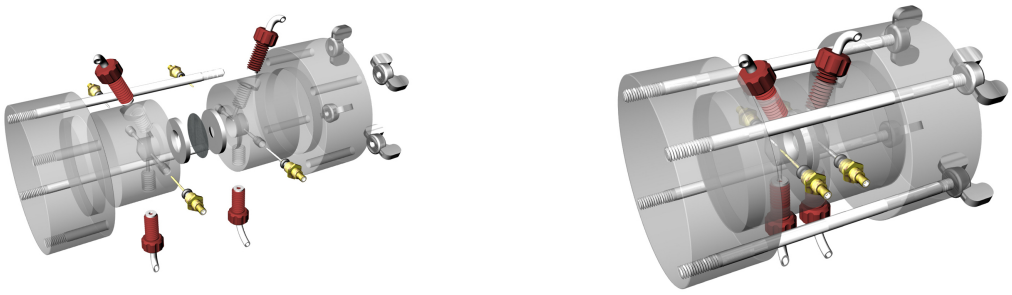

Figure 2.17: *Cartoon of custom-made cell.*

2.3.3 Custom-made cell

Experimental measurements were performed in a custom-made cell, constinting of two Teflon blocks (called bi-cell) kept in place by two Perspex cups connected by three screws.[3] The polycarbonate membrane was housed between the two Teflon blocks, leaving exposed a circular surface of $19.6mm^2$. The bi-cell made by G. Favero et al. 2002[3] was modified in the chemistry department (Univrsity of Florence)as described in Figure 2.17: both the two Ag/AgCl electrodes and the Au electrodes were present in the same working cell, outlet tubes were skewed in order to inject external solution in proximity of the membrane surface, the volume was reduced from 2ml to $400\mu l$ and the external wall was made of plexiglass in order to observe air bubble formation.

2.3.4 Experimental set up

The device was placed in a Faraday cage, which was set on an antivibrating support to reduce electromagnetic and electrostatic interference during measurements. To control temperature the working cell was placed in a termostatated chamber settled at 25°C during conductivity measurements. In electrochemical measurements potentials were measured versus Ag/AgCl electrodes. Gold electrods were used for conductivity measurements.

2.4 Peptide-Proteins Incorporation

Gram D ($25\mu M$) and Tricogin ($4\mu M$) in ethanol solution were embedded by simple diffusion, Gramicidin and Trichogin were added in the Tris buffer through the outlet tube in order to reach the proximity of the membrane, when the nanoBLMs were already formed. Phospholamban was embedded by using vesicles fusion. A $3:1:1$ mass ratio mixture of DOPC:Cholesterol:PLN was dried from the respective solvent, resuspended in TRIS-HCl buffer $10mM$, pH=7.5, sonicated for 10 minutes and pipetted onto a Isopore membrane filter with $0.4\mu m$ pore size (Millipore) held in a Swinnex plastic cartridge (Millipore) affixed to a 3ml plastic syringe to form small unilammellar vesicles (SUV). The obtained vesicles solution was diluted by TRIS buffer and added to the cis compartment using the peristaltic pump. In the mean time TRIS buffer was introduced in

the trans compartment in order to have the same hydrostatic pressure in both compartments to avoid membrane breaking.[25]

Chapter 3

Results and Discussion

3.1 Supported membrane formation

3.1.1 Polycarbonate filter

Polycarbonate filter is the main support of nanoBLMs. During this research it has been noticed that to obtain good nanoBLMs, the weight of the filter has to be $\backsim 0.1 mg/cm^2$ (that correspond to a thickness of $\backsim 10 \mu m$). Moreover the surface has to be smooth and the pores regular in diameter size.

3.1.2 Gold deposition

Gold deposition is one of the most tricky step. The first condition for high quality gold deposition is that the vacuum chamber in the AGAR Automatic Sputter Coater has to be clean and without contamination of any other metal. Two procedures were tested for gold deposition; one characterized by a fast deposition rate (obtained using the following parameters: Current $40 mA$, Time $120 s$, Pressure $0.08 * 10^{-1}$ mbar) and the other one charaterized by a slow deposition rate (obtained using the following parameters: Current $20 mA$, Time $150 s$, Pressure $2 * 10^{-1}$ mbar). It came out that the parameters utilized for gold deposition rate are important, and in particular a slower deposition rate is more efficient than a faster one. Results are reported in EIS paragraph 3.2.3.

3.1.3 SAM-ODT formation

Formation of self-assembled octadecanethiol monolayer (SAM-ODT) is a simple step. We usually spread 100 μl of an ethanolic solution of $3 mM$ octadecanethiol on the polycarbonate filter surface for about 10 minutes. After ODT incubation the filter was washed in ethanol and water and then dried by a nitrogen flow. Before and after SAM-ODT formation, specific resistance and specific capacitance values remained constant (data reported in Table 3.1). It means that the pores present in the supported membranes are not occluded by ODT and they maintain the original size. These data are in agreement with an AFM picture reported in Favero et al. 2002,[3] where it appears clear that ODT monolayer does not obstruct the pores of the supported filters.

support	R	C
Poly-Au	$0.28K\Omega cm^2$	$0.11\mu F/cm^2$
SAM-ODT	$0.38K\Omega cm^2$	$0.22\mu F/cm^2$
nanoBLMs	0.1-$50M\Omega cm^2$	0.423-$0.77\mu F/cm^2$

Table 3.1: *Specific resistance and Specific capacitance values recorded on polycarbonate filter coverd by gold (Poly-Au), SAM-ODT and nanoBLMs. For nanoBLMs a range of values is reported because of the high variability (30 samples).*

3.2 nanoBLMs characterization

NanoBLM is a system able to combine long-lasting mechanical stability with the biomimetic properties of the traditional BLM. Moreover, in nanoBLMs it is possible to carry out measurements under costant perfusion. During this research project nanoBLMs were characterized using different techniques on the same support. A range of values for each parameter were detected in order to identify suitable nanoBLMs. The importance of characterizing a new experimental model is to have a method to identify suitable nanoBLMs to carry out reliable experimental measurements. After nanoBLMs formation, an increase of specific resistance and specific capacitance values was observed, as reported in Table 3.1.

3.2.1 CV voltammetry

CV voltammetry was used to obtain specific resistance value of the membranes, as described in paragraph 2.2.2. In Figure 3.1 the voltammograms before adding lipids (dashed line) and after nanoBLMs formation (solid line) are shown.

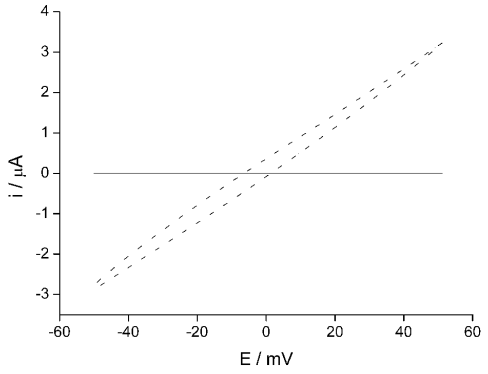

Figure 3.1: *Cyclic voltammograms for SAM-ODT (dashed line) and nanoBLMs (solid line).*

After nanoBLMs formation, the specific resistance increases significantly, up to 4 order of magnitude (from $0.32K\Omega cm^2$ to $2M\Omega cm^2$, in the example shown in Figure 3.1). The specific resistance value for nanoBLMs is highly variable, and

it usually ranges between 0.12 and $34 M\Omega cm^2$ (data obtained by analyzing 30 samples).

3.2.2 AC voltammetry

Specific capacitance values can be obtained by AC voltammetry, as described in paragraph 2.2.3. Usually the nanoBLM was characterized by both CV and AC techniques.

Since the specific capacitance increases from $0.12 \mu F/cm^2$ to $0.43 \mu F/cm^2$, after nanoBLMs formation, it is evident that the pores present in the support are covered by the phospholipid bilayer. The specific capacitance value for nanoBLMs usually ranges between 0.3 and $0.77 \mu F/cm^2$ (data obtained by analyzing 30 samples).

3.2.3 EIS

EIS is an electrochemical technique used to characterized the nanoBLMs. Specific resistance and specific capacitance values were determined as described in paragraph 2.2.4. Figure 3.2 shows a Bode plot recorded on the same nanoBLMs characterized by AC and CV technique.

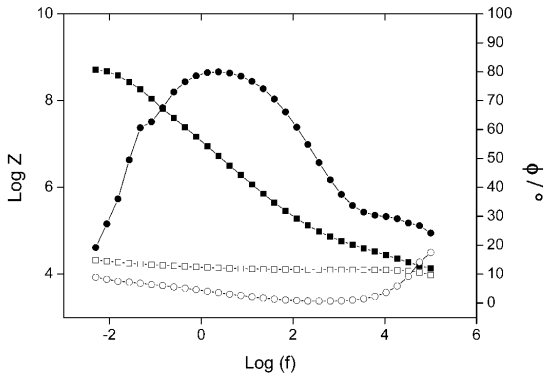

Figure 3.2: *Logarithm of the impedance, Z (square symbol) and phase, ϕ (circle symbol) vs. logarithm of the frequency (f): curves recorded on nanoBLMs (filled symbol) and SAM-ODT (empty symbol). All data were obtained at zero offset potential. 10mM TRIS-HCL buffer pH = 7.5 was present into working cell compartments.*

The impedance spectrum is characterized by the electrolyte resistance R_{el} in the high frequency region over 10^4 Hz. At frequencies below 10^4 Hz the phase angle and the impedance are due to the capacitance C_m related to the membrane. At frequencies below 10^{-1} Hz, a second ohmic resistance is detected, which is attributed to the membrane resistance R_m. The EIS data were fitted using the equivalent circuit shown in Figure 2.13. A strong increase of specific resistance (up to a factor of 10^4 order of magnitude $0.11 K\Omega cm^2$ and $8.17 M\Omega cm^2$)is recorded after nanoBLMs formation. The specific capacitance increased slightly (1 order

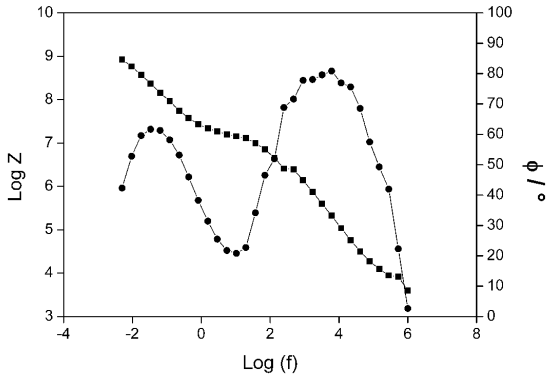

Figure 3.3: *Logarithm of the impedance, Z (square symbol) and phase, ϕ (circle symbol) vs. logarithm of the frequency (f): curves recorded on nanoBLMs (filled symbol). All data were obtained at zero offset potential. 10mM TRIS-HCL buffer ($pH = 7.5$) was present into the working cell compartments.*

of magnitude $0.028\mu F cm^{-2}$ and $0.68\mu F cm^{-2}$). The supported membrane characterized was obtained by a slow deposition rate (sputtering parameters: Current $20mA$, Time $150s$, Pressure $2 * 10^{-1}$ mbar). In Figure 3.3 it is shown the Bode plot recorded on nanoBLMs formed on a polycarbonate filter covered by gold at a high deposition rate (sputtering parameters: Current $40mA$, Time $120s$, Pressure $0.08 * 10^{-1}$ mbar). The equivalent circuit, that was fitted to the experimental data (shown in Figure 3.3), is composed of two parrallel RC-meshes in series to an ohmic resistance. Since the phospholipid bilayer can be described with a RC mesh, the presence of two phase peaks means that two regions characterized by two different time costants are present. We may conclude that the phospholipid bilayer is not homogeneous and defects are probably present in the nanoBLMs. Unfortunately this technique does not allow us to localize the defects.

3.2.4 Conductivity

Bilayer characterization was also performed by conductivity measurements. In Figure 3.4 the conductivity values for SAM-ODT and nanoBLMs are reported. After nanoBLMs formation, the conductivity is lower than in the presence of SAM-ODT and it is not dependent on the electrolyte concentration in the bicell. This data are in agreement with data reported in Favero et al. 2002,[3] where membrane formation was monitored by conductivity measurements.

3.2.5 Discussion

Characterization of nanoBLMs by means of electrochemical and conductivity measurements allows us to estimate when good nanoBLMs are formed. On the basis of data obtained from at least 30 samples, the ranges for each parameter have been determinated. In the presence of nanoBLMs, specific resistance values obtained by different techniques, e.g. CV and EIS, have to be similar and they

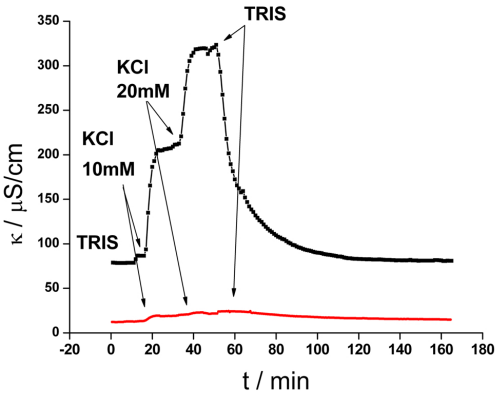

Figure 3.4: *Conductivity vs. time, recorded on SAM-ODT (black) and on nanoBLMs (red). Data were collected under constant perfusion (2ml/min). The experiment started with 10mM TRIS-HCL buffer, pH = 7.5 in the bicell. The solution was exchanged by adding to the bicell compartments TRIS plus KCl at two different concentrations (10mM and 20mM) in 10mM TRIS-HCl buffer, pH=7.5.*

are included in a range between 0.1 and $50M\Omega cm^2$. The high variability observed in specific resistance is probably due to the ammount of solvent present in the bilayer and the total area of nanoBLMs. The specific capacitance measured by AC Voltammetry is usually lower than the one determined by EIS. The values obtained by the two techniques should be in the same order of magnitude. The range detected for nanoBLMs measured by AC voltammetry is between $0.23\mu Fcm^{-2}$ and $0.77\mu Fcm^{-2}$. The specific capacitance obtained by EIS measurements usually ranges between $0.4\mu Fcm^{-2}$ and $1.4\mu Fcm^{-2}$. Conductivity values for nanoBLMs are included in between $6.9\mu Scm^{-1}$ and $39\mu Scm^{-1}$. Probably in a bilayer characterized by high resistance a low ammount of molecules can be embedded in the membrane. It is difficult to control the quantity of proteins or peptides embedded in experimental biomimetic models because the incorporation process is unclear.

3.3 Embedding in nanoBLMS

During this research project different protocols of incorporation were tested using three molecules: i)Gramicidin, which can forms selective pores; ii)Trichogin, whose channel activity is still unknown; iii)Phospholamban, whose channel activity is matter of debate.

3.3.1 Gramicidin

To check the reliability of our new system we test Gramicidin, which has already been embedded in nanoBLMs by Favero et al. 2002.[3] Gramicidin was added at one side of the membrane and in its proximity at final concentration of $25\mu M$. Specific resistance and specific capacitance values were recorded to verify

the integrity of the membrane and the incorporation of Gramicidin. Subsequently, conductivity measurements were carried out on the same membrane, where the peptide was successfully incorporated.

In Figure 3.5 the Bode plot recorded on nanoBLMs before and after Gramicidin incorporation, is reported.

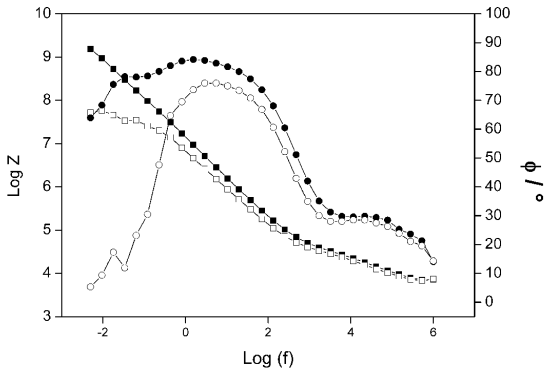

Figure 3.5: *Logarithm of the impedance, Z (square symbol) and phase, ϕ (circle symbol) vs. logarithm of the frequency (f): curves recorded on nanoBLMs (filled symbol) and on nanoBLMs containing Gramicidin after* 20 *hours(empty symbol). All data were obtained at zero offset potential. 10mM TRIS-HCL buffer pH* = 7.5 *was present into the working cell compartments.*

By fitting the equivalent circuit (Figure 2.13) to the data reported in Figure 3.5 we observe a decrease in resistance by a factor of 10^2 order of magnitude after Gramicidin addition, which suggests a successful incorporation and the presence of pores ($43.7 M\Omega cm^2$ and $0.69 M\Omega cm^2$, before and after Gramicidin addition, respectively). The fact that approximately the same capacitance value was recorded in the absence and presence of Gramicidin proves the integrity of the membrane ($0.64 \mu F cm^{-2}$ and $1 \mu F cm^{-2}$, respectively). Indeed, it is well known that channel formation by peptides or small proteins in biomimetic models causes a decrease in specific resistance.[27,28] On the same system conductivity measurements were carried out to check ion selectivity. Data, reported in Gualdani 2006,[29] confirm data published in Vallejo and Gervasi, 2002 and Favero et al. 2002.[3,4]

3.3.2 Trichogin

The same procedure was adopted to analyze Trichogin. Trichogin was added at one side of the membrane and in its proximity at a final concentration of $2 \mu M$. Figure 3.6 shows the Bode plot recorded on nanoBLMs before and after Trichogin incorporation.

By fitting the the equivalent circuit (Figure 2.13) to the data of Figure 3.6 we obseve a decrease in resistance associated with Trichogin incorporation, (7.6 $M\Omega cm^2$ and $12.5 K\Omega cm^2$, before and after Trichogin incorporation, respectively). Similar values for specific capacitance value were recorded in the absence and presence of Trichogin (0.35 and $0.99 \mu F cm^{-2}$, respectively). After Trichogin was

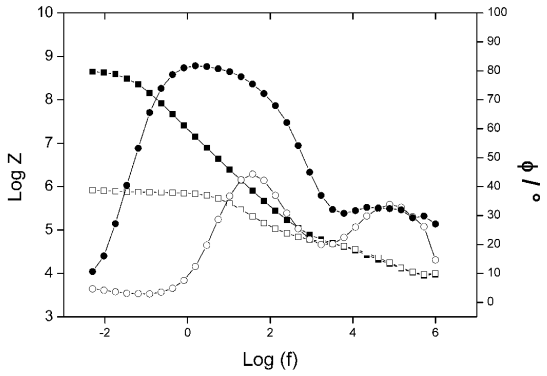

Figure 3.6: *Logarithm of the impedance, Z (square symbol) and phase, ϕ (circle symbol) vs. logarithm of the frequency (f): curves recorded on nanoBLMs (filled symbol) and on nanoBLMs containing Trichogin after* 3 *days (empty symbol). All data were obtained at zero offset potential. 10mM TRIS-HCL buffer pH* = 7.5 *was present into the working cell compartments.*

embedded in the nanoBLMs conductivity analysis was carried out. In Figure 3.7 the conductivity recorded on Trichogin embedded in nanoBLMs is shown. Our data show that Trichogin can form pores, which allow K^+ and Cl^- to pass through it.

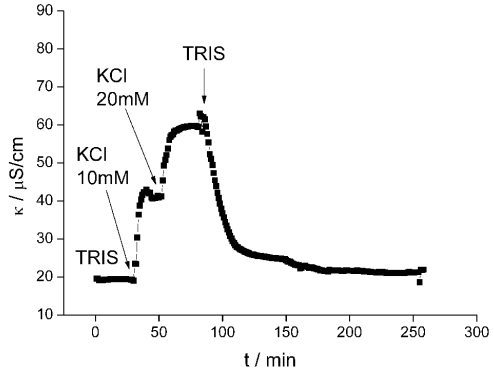

Figure 3.7: *Conductivity vs. time, recorded on nanoBLMs containing Trichogin. Data were collected under constant perfusion (*2*ml/min) of bicells. The experiment started with* 10*mM TRIS-HCL buffer, pH* = 7.5 *in the bicell. The solution was exchanged by flowing into bicell compartments TRIS plus KCl at two different concentrations (*10*mM and* 20*mM) in* 10*mM TRIS-HCl buffer, pH=*7.5*.*

A second procedure was used to verify Trichogin incorporation. In this case Trichogin incorporation was monitored by conductivity measurements. Conductivity (Figure 3.8) was recorded continuosly and under costant perfusion. The experiment started with a background buffer solution ($10mM$ TRIS-HCL buffer, $pH = 7.5$) in the bicell. Trichogin was added at $16\mu M$ during the measurements. An instantaneous increase in conductivity was observed, indicating Trichogin in-

corporation in the membrane. After Trichogin incorporation, the solution was exchanged by flowing into the bicell compartments TRIS plus KCl at two different concentrations ($10mM$ and $20mM$) in $10mM$ TRIS-HCl buffer, $pH = 7.5$. To check the reversibility of our system, after each electrolyte addition the background solution was once again perfused into the bicell. A strong increase of conductivity was recorded in the presence of $10mM$ KCl. In the presence of $20mM$ KCl, the conductivity doubled the value recorded in the presence of KCl $10mM$.

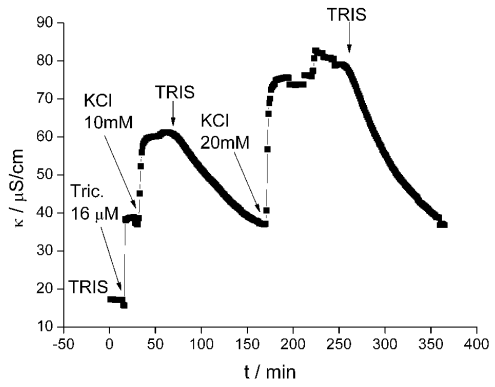

Figure 3.8: *Conductivity vs. time, recorded on nanoBLMs. Data were collected under constant perfusion ($2ml/min$) of bicells. The experiment started with only $10mM$ TRIS-HCL buffer, $pH = 7.5$ in the bicell. $16\mu M$ Trichogin was added to the bicell during the measurements. The solution was exchanged by flowing into the bicell compartments TRIS or TRIS plus KCl at two different concentrations ($10mM$ and $20mM$) in $10mM$ TRIS-HCl buffer, $pH = 7.5$.*

3.3.3 PLN

PLN is too long and very hydrophobic to be incorporated at a high ammount of molecules from acqueous solution by simple diffusion. Therefore a vesicle fusion protocol was used. Vesicles containing PLN were characterized by a 3:1:1 mass ratio mixture of DOPC :Cholesterol:PLN. Specific resistance and specific capacitance values were recorded by performing EIS measurements to verify the integrity of the membrane and PLN incorporation as shown in Figure 3.9; subsequently conductivity measurements were carried out on the same membrane, where PLN was successfully incorporated. The respective values were obtained by fitting an equivalent circuit (Figure 2.13) to the experimental data presented in Figure 3.9. Data obtained with and without PLN show the same order of magnitude for the specific capacitance (1.4 and $1.3\mu Fcm^{-2}$ before and after PLN incorporation, respectively) and a decrease in the specific resistance by a factor of 10^4 after PLN incorporation ($30.4M\Omega cm^2$ and $5.4K\Omega cm^2$ before and after PLN incorporation, respectively).

Capacitance values obtained by fitting the equivalent circuit to the experimental EIS data were compared with the ones obtained by AC (0.55 and $0.86\mu Scm^{-1}$

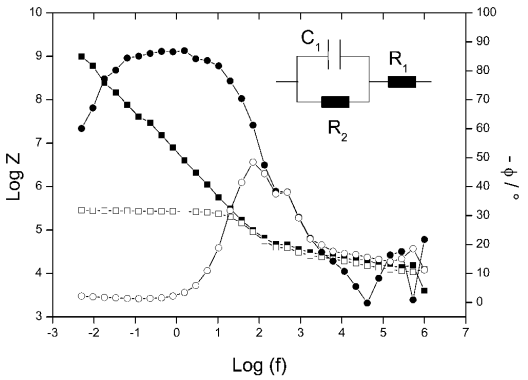

Figure 3.9: *Logarithm of the impedance, Z (square symbol) and phase, ϕ (circle symbol) vs. logarithm of the frequency (f): curves recorded on nanoBLMs (filled symbol) and on nanoBLMs containing PLN after* 3 *days (empty symbol). All data were obtained at zero offset potential. 10mM TRIS-HCL buffer pH* = 7.5 *was present into working cell compartments.*

before and after PLN incorporation, respectively). Data are in good agreement.

Conductivity measurements were started with a background electrolyte before different electrolyte solutions (at two different concentration levels) were allowed to flow ($2ml/min$) through both cell compartments. As background electrolyte a $10mM$ TRIS-HCL buffer ($pH = 7.5$) solution was used; after a constant conductance value was reached, this buffer was replaced by a solution containing the background electrolyte plus a fixed concentration ($10mM$ and $20mM$) of a suitable electrolyte, i.e. KCl, $NaClO_4$ and ChoCl (choline chloride). To check the system reversibility, after each electrolyte the background solution was once again perfused into the bicell.

Figure 3.10 reports the conductivity value vs. time for nanoBLMs embedding PLN in response to different electrolyte solutions. The data show that the conductivity value of nanoBLMs containing PLN increased when different electrolytes where perfused through the chamber.
The different tested electrolytes where chosen in such a way to make evident the contribution of different ions to the whole conductivity. In particular, the different recorded conductivity between $NaClO_4$ and NaCl (at the same concentration) can be justified simply on the basis of equivalent conductance values of Cl^- and ClO_4^- (equivalent conductance at infinite dilution is 76.3 and $67.3 Scm^2eq^{-1}$, respectively) since the Na^+ contribution is the same. Moreover useful information about PLN may be obtained by comparing ChoCl and NaCl conductivity values. By considering the equivalent conductance at infinite dilution of NaCl ($126.4 Scm^2eq^{-1}$) Cl^- contributes for ca. 60% of the total recorded conductivity. Thus, for ChoCl the expected conductance is 60% of that NaCl at the same concentration if also Cho^+ contribute to the signal. Since the conductance of ChoCl is around 60% of that of NaCl, it is evident that Cho^+ does not give an appreciable contribution to the whole recorded conductance signal. These results suggest that PLN is permeable only to relatively small ions as Na^+, Cl^- and

ClO_4^- while bigger ions as Cho^+ are unable to pass trough it.

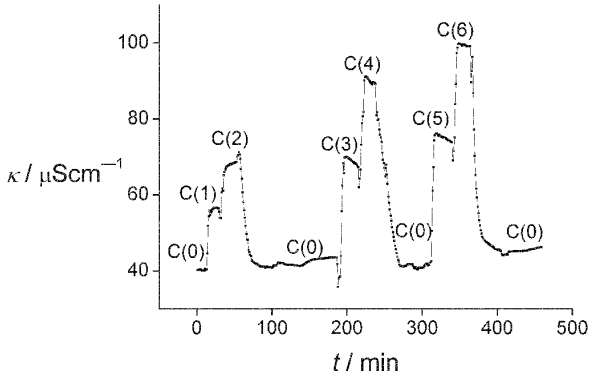

Figure 3.10: *Conductivity vs. time, recorded on PLN embedded in nanoBLMs by vesicles fusion. Data were collected under constant perfusion (2 ml/min) of bicells. Experiment started with only* $10mM$ *TRIS-HCL buffer,* $pH = 7.5$ $[C(0)]$ *in the bicell. The solution was exchanged by flowing into bicell compartments TRIS plus one of the following electrolyte: ChoCl,* $NaClO_4$ *and NaCl at different concentration [C(1)=ChoCl* $10mM$*, C(2)=ChoCl* $20mM$*, C(3)=* $NaClO_4$ $10mM$*, C(4)=* $NaClO_4$ $20mM$ *C(5)= NaCl* $10mM$*, C(6)= NaCl* $20mM$*] in* $10mM$ *TRIS-HCl buffer,* $pH = 7.5$*.*

Our data together with literature ones[9,30] are consistent with the hypothesis that the pentameric PLN can form non-selective ion conducting pores. Based on their model of a bellflower structure, Oxenoid and Chou suggested that many physiologically relevant ions such as Na^+, K^+, Ca^{2+} and Cl^- are small enough to pass through the narrowest part of the pentamer PLN (diameter $\approx 3.6\mathring{A}$). In agreement with the latter model the Cho^+ cation (radius $3.3\mathring{A}$[31]) was found not to be conducted, because it is larger than the estimated PLN pore.[9]

3.4 PLN embedded in traditional BLMs

To further test the channel forming ability of PLN, the same protein was incorporated in traditional BLM for single channel recordings (experiments carried out at the TUDarmstadt University). As in this case a low amount of molecules is enough to see single channel event, PLN was added in solution at a final concentration of $0.3\mu M$ (PLN was solubilized in water after liophylization). Before adding the protein, the bilayer conductance was recorded for approximately 1 hour in order to exclude artefacts from contaminations. Only bilayer without artefacts were used for recostitution of PLN. Figure 3.11A shows some representative recordings from these experiments revealing typical current fluctuations between a closed and a defined opening state. Figure 3.11C illustrates a plot of the unitary open channel currents measured under symmetrical conditions ($500mM$ KCl) as a function of voltage. The I/V relation is linear, reverses at $0mV$ and has a slope conductance of $27pS$. Often an additional smaller conductance was

found together with the larger $27pS$ conductance.

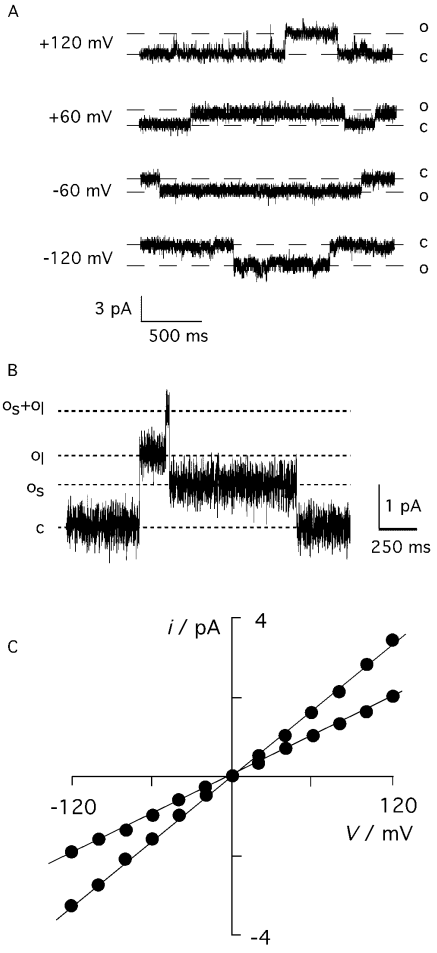

Figure 3.11: *PLN generates single channel fluctuations in planar lipid bilayer.(A) Single channel activity recorded at different holding potentials, from* $-120mV$ *to* $120mV$ *in symmetrical solution with* $500mM$ *KCl in* $10mM$ *MOPS/TRIS (pH* $= 7$*) buffer. c and o refer to the closed and open states of the channel, respectively.(B) Example of concomitant opening/closing of large conductance and small conductance. The two events are additive. First the large conductance opens (ol) before also a lower conductance opens (os). Together the current reaches the sum of both amplitudes (ol+os). Upon closing of the large conductance the current reaches the amplitude of the small conductance. Closing of the small conductance brings the current back to the baseline (c).(C) Current/voltage relation of large and small unitary currents obtained in same conditions as in A and B.*

Figure 3.11B shows an example for the independent opening/closing of the two different conductances. In the example trace obtained at $60mV$ holding voltage the small conductance is opening on top of the large conductance; both conductances close in opposite sequence. The fact that the two conductances are like in the example always additive means that the low conductance is not a sub-conductance level of the larger one. An I/V plot (Figure 3.11C) of the small unitary channel fluctuations again reveals a linear relation, which reverses

at $0mV$ and has a conductance of $16pS$. To obtain information on the basic functional parameters of the large and small conductance the channel fluctuations were fitted by the QuB algorithm.[32] Good fits could be achieved assuming a simple o-c model. For a reference voltage of +80mV this procedure yields an open probability (P0) of 0.5 and 0.1 for the large and the small conductance, respectively. The mean open dwell times were 680 ms and 560 ms for the large and small conductance, respectively. The open probability and the relatively long open channel dwell times look similar to those reported previously for PLN channel activity.[30] Indeed also in previous experiments[30,33] small unitary channel fluctuations with two different conductances were observed upon reconstituting full length PLN or the c-terminal fragment (amino acids 26 - 52) in lipid bilayers. Worth noting is that the present data and the previous recordings were obtained with different bilayer techniques and in different lipids;[30,33] this stresses the fact that the channel events recorded with PLN are due to the protein and not to a bilayer artefact.

3.5 Discussion

Since techniques such as electrochemical and conductivity recordings measure macro currents, high quantity of molecules have to be embedded in the bilayer to detect any effect. On the contrary in single channel measurements, where pA currents are recorded, a small amount of molecules is sufficient to generate single channel events. Gramicidin and Trichogin are small enough, to be embedded in the nanoBLMs by adding them in solution. Concerning PLN, in our opinion an insufficient amount of molecules were incorporated into the membrane. We solved this problem by fusing vesicles containing PLN with nanoBLMs. On the other hand, for single channel recordings an adequate number of PLN molecules was embedded in the BLMs by simple diffusion.
Gramicidin was used to test the reliability of nanoBLMs. Since selectivity data about Gramicidin present in literature were confirmed,[3,4,29] nanoBLMs were considered a suitable system to detect pore formation in membranes in the case of short peptides. In this work Trichogin and Phospholamban were studied; the function and the mechanism of action of both molecules are still unknown. During this research project, attention was focused on whether the two molecules can form pores or ion channels into the membrane.

- Data obtained from conductivity measurements in the presence of Trichogin indicate that Trichogin may form membrane pores in this biomimetic model. This hypothesis is supported by electrochemical data,[34] data obtained by fluorescensce spectroscopy and fluorescence quenching experiments[35] and recent molecular dynamics (MD) simulations.[36] General mechanisms describing formation of membrane pores by antimicrobial peptides can be found in Brogden 2005.[6] One of the first hypothesis, i.e. the barrel-stave mechanism, was proposed more than 30 years ago but his validity was confirmed only for the peptaibol alamecitin.[36] Alamecitin is longer than Trichogin (20 residues) and it can span the thickness of the bilayer. Since the

length of Trichogin in its helical conformation is only about half the normal thickness of a lipid bilayer, this peptaibol is too short to fully span a membrane. It was supposed that its mechanism of action had to be different from the long peptaibols, like alamethicin forming voltage-gated channel. However, the MD simulations presented in Bocchinfuso et al. 2005[36] suggested that "trichogin GA IV, when inserted in a transmembrane orientation, causes a significant thinning of the bilayer, and it might thus be able to be in contact with both membrane surfaces at the same time. Therefore, a normal barrel-stave arrangement, with the peptide chains aggregated laterally to form a cylinder superstructure, the inner water-filled lumen of which is lined by the hydrophilic sides of the helices, could be sufficient to describe the mechanism of pore formation even for such a relatively short peptide".[36] Our data support this hypothesis as incorporation of Trichogin embedding in nanoBLMs was carried out by adding the peptaibol in solution at one side of the membrane.

- In order to understand if PLN pentamer can have ion channel activity, we have performed experiments by using two different biomimetic systems namely supported nanoBLMs and traditional black lipid membranes, BLMs; both systems are characterized by the lipid bilayer membrane(s) separating two compartments (cis and trans) containing aqueous solutions. These experimental systems are suitable for mimicking at the best the intra- and the extra- cellular sides of a biological membrane. The following results, which were obtained by the two complementary approaches, show that PLN conducts ions across a lipid bilayer by an inherent ion channel activity.

Chapter 4

Conclusions

"Can Phospholamban form ion channels?" was the main question that drove me in thess three years of the PhD research project. Structure and function of the pentameric form of PLN are still controversial issues in the literature. In order to understand if PLN pentamer can have ion channel activity, we have performed experiments by using both conductivity measurements in nanoBLMs and single channel recordings in traditional black lipid membranes, BLMs. The two different techniques are complementary and so the agreement of data obtained from both the techniques prove the reliability of the results. NanoBLMs are a new biomimetic system, which can be used to study the selectivity of ion channels. NanoBLMs were developed to overcome the fragility of traditional BLMs, because they are characterized by a long-lasting mechanical stability. This feature allows to carry out measurements for days and under costant perfusion. Moreover the new custom made cell is provided with two kinds of electrodes, Ag/AgCl and gold electrodes, which allow to obtain complementary information from different techniques on the same membrane. The disadvantage of this technique is that a high density of active channels is required in order to observe a signal. On the contrary single channel recordings allow to detect the activity of a few molecules incorporated in the model membrane. In conclusion we developed a new experimental membrane model useful to detect pore formation and ion channel selectivity. Conductivity data support the view that PLN functions as an ion channel. Our results were confirmed by single channel recordings. The demonstration of channel function of PLN is of great interest as it can be involved in the regulation of cardiac contraction-relaxation. Moreover PLN could be a promising therapeutic target against heart failure and other cardiac diseases.

Acknowledgements

I would like to thank all the people who made this work possible. Prof.M.R. Moncelli, Dr. F. Tadini, Dr. G. Bartolommei, Dr. C. Guidotti, A. Pozzi, A. Sacconi and R. Gualdani from Bioelectrolab, Chemistry Department University of Florence; Dr. S. Caporali from University of Florence, Prof. G. Rispoli from University of Ferrara, Prof. T. Ferri University "La Sapienza" Rome, Prof. G. Thiel and M. Henkel from TUDarmstadt University, Prof. A. Moroni from University of Milan, Prof. G. Inesi from California Pacific Medical Center, San Francisco.

Chapter 5

Appendix

In this Appendix two published abstracts and a submitted paper are reported. The first abstract, published in *FEBS Journal 275 (Suppl 1), 358 (2008)*, concerns the preliminary study of Trichogin in nanoBLMs. The second abstract was selected for an oral presentation at the 9th Young Scientist Forum and 34th FEBS Congress Praga (2-9 July 2009) and is published in *FEBS Journal 276 (Suppl 1), 390 (2009)*. In this abstract conductivity results about PLN are described. The manuscript is submitted to FEBS Letters. It reports the results on PLN obtained by conductivity and single channel recordings and the concerning discussions.

PP7-35

Behaviour of the peptaibol trichogin in a mixed hybrid bilayer lipid membrane array (nanoBLMs)

S. Smeazzetto[1], T. Ferri[2] and M. R. Moncelli[1]
[1]*Dipartimento di Chimica, Universitá di Firenze, Florence, ITALY*
[2]*Dipartimento di Chimica, Universitá di Roma 'La Sapienza', Rome, ITALY*

Introduction: The peptaibols are a family of antibiotic peptides isolated from soil fungi that exhibit anti-bacterial and anti-fungal properties. The name peptaibol derives from their chemical composition: peptides containing Aib (α-amminoisobutyric acid or α-methyl alanine) residues and ending in a C-terminal alchol. Trichogin is one of the shortest peptaibols (11 residues) and it has a fatty acyl moiety linked to the N-terminal amino acid (n-octanoyl). Trichogin is too short to fully span a membrane, so its mechanism of action must be different from the long peptaibols, like alamethicin forming voltage-gated channel.

Methods: We are studying these peptaibols using a new experimental model of biological membrane [1]. This model is constituted of a polycarbonate membrane with 1 μm diameter holes, covered by an octadecanthiol (ODT) self-assembled monolayer (SAM) on Au. The bilayer lipid membranes (BLMs) spontaneously self-assemble on the holes of the polycarbonate membrane. The characterization and stability of the nanoBLMs have been characterized by electrochemical measurements: cyclic voltammetry, AC voltammetry and Impedance Spectroscopy.

Results: We identified the typical range of values of specific resistance, specific capacitance and conductance for well formed nanoBLMs: $0.1 M\Omega < R*cm^2 < 10$ MΩ $0.4 microF < C/cm^2 < 1 microF$ and $0 < \kappa < 5$ microS/cm respectively. By means of specific resistance data, we furthermore proved that nanoBLMs can last up to 24 hours.

Conclusion: We set up the protocol to incorporate the trichogin in the phospholipidic bilayer and to study its selectivity.

Reference:

1. Favero *et al., Acta* 2002; **460**: 23–34.

YSF–99
Study of phospholamban incorporated in nanoBLMs

S. Smeazzetto[1], T. Ferri[2] and M. R. Moncelli[1]
[1]*Department of Chemistry, University of Florence, Sesto Fiorentino Florence, ITALY,* [2]*Department of Chemistry, University of Rome 'La Sapienza', Rome, ITALY*

Background: Phospholamban (wt-PLN) is an integral membrane protein that regulates cardiac sarco/endoplasmatic CaATPase (SERCA). PLN exists in equilibrium between monomeric and pentameric forms. Monomeric unphosphorylated PLN inhibits SERCA, but when PLN is phosphorylated releases the inhibition and allows calcium translocation. In literature there are four principal proposed structural models of pentameric wt-PLN (1) and it is not clear if the wt-PLN pentamer can form membrane pores.

Methods: We are studying PLN using a new experimental model of biological membrane (nanoBLMs) (2). The properties of the nanoBLMs have been characterized by conductivity and electrochemical measurements.

Results: The conductivity recorded on nanoBLMs containing wt-PLN in the presence of $NaClO_4$ is ~90% of the value in the presence of NaCl. This result is in agreement with the values of equivalent conductance at infinite dilution for Cl^- and ClO_4^-. Moreover it is evident that the conductance in the presence of ChoCl is half of that of NaCl at the same concentration. These results suggest that contrary to Na^+, Cl^- and ClO_4^-, Cho^+ cannot pass through the membrane embedding wt-PLN.

Conclusion: From our experimental data it seems that wt-PLN can form pores which are not selective for small ions. These data are in agreement with the hypothesis of Oxenoid and Chou (3), according to which physiologically relevant ions such as Na^+, K^+ and Cl^- are small enough to pass through the narrowest part of the wt-PLN pentamer (diameter ~ 0.36 nm). This pore dimension is supported by our experimental data indicating that a big organic cation like Cho^+ (radius 0.33 nm) cannot pass through the membrane containing wt-PLN.

References:

1. Favero, *et al., J Am Chem Soc.* 2005; **127(22)**:8103.
2. Traaseth, *et al., Proc Natl Acad Sci* USA. 2007; **104(37)**:14676.
3. *Proc Natl Acad Sci* USA. 2005; **102(31)**:10870.

Ion channel activity of pentameric Phospholamban

Serena Smeazzetto[a], Michael Henkel[b], Tommaso Ferri[c], Gerhard Thiel[b], Maria Rosa Moncelli[a]

[a] Dipartimento di Chimica, Università di Firenze, Via della Lastruccia 3, 50019 Sesto Fiorentino, Firenze (Italy), e-mail: serena.smeazzetto@unifi.it, moncelli@unifi.it

[b] Institute of Botany, Technische Universität Darmstadt, Schnittspahnstrasse 3, 64287 Darmstadt (Germany), e-mail: henkel@bio.tu-darmstadt.de, gerhardthiel@me.com,

[c] Dipartimento di Chimica, Università "La Sapienza" di Roma, Piazza Aldo Moro 5, 00185 Roma (Italy), e-mail: tommaso.ferri@uniroma1.it

Corresponding author: Maria Rosa Moncelli[a] e-mail: moncelli@unifi.it, Dipartimento di Chimica, Università di Firenze, Via della Lastruccia 3, 50019 Sesto Fiorentino, Firenze (Italy) Tel: (+39 055 4573100) Fax: (+39 055 4573142).

Abstract

Phosholamban (PLN) is involved in the contractility of cardiac muscle by regulating intracellular calcium concentration (Ca^{2+}_{cyt}) of cardiac myocytes. PLN is regulator of sarco/endo plasmic CaATPase (SERCA) but concerning his structure and activity many questions are still open. In the present paper we focused our attention on the main issue whether the more stable pentameric form is an ion channel or simply a storage form. We used two different biomimetic systems namely supported nanoBLMs and traditional black lipid membranes, BLMs supporting the view that PLN works as an ion channel.

Keywords: Bilayer lipid membranes; Ion channel; Membrane proteins; Phospholamban

Abbreviations: PLN, phospholamban

1 Introduction

Phospholamban (PLN) is a 52 amino acids, integral membrane protein, which is involved in the contractility of cardiac muscle by regulating the intracellular calcium concentration (Ca^{2+}_{cyt}) of cardiac myocytes. PLN modulates Ca^{2+}_{cyt} by regulating the cardiac sarco/endoplasmatic CaATPase (SERCA). This membrane protein in the sarcoplasmic reticulum (SR) maintains a low intracellular calcium concentration by pumping Ca^{2+} into the SR. Activity of SERCA is inhibited by the unphosphorylated PLN whereas phosphorylated PLN releases SERCA inhibition and allows pumping of calcium. PLN monomer (6KDa) is in an equilibrium with its pentameric form[1]; the more stable pentamer is a 30KDa oligomer in which each monomer is composed of three domains: a helical cytoplasmic domain, a semi-flexible loop and a helical hydrophobic transmembrane domain[2, 3]. Various details on the structure of PLN and its activity are still a matter of debate. It is not known whether the interaction with SERCA is due to the monomeric or pentameric form[4-6]. Also structural details of the PLN pentamer are not yet rectified and currently a so called bellflower model[2] and a pinwheel model[7] of the pentamer are discussed in the literature [2, 7-9]

In this paper we focused our attention on the main issue whether the more stable pentameric form is an ion channel or simply a storage form. A combination of functional studies[10], mutagenesis[11, 12] , structural studies[2, 13] and molecular modelling[14] support the hypothesis that PLN can indeed have a transmembrane orientation with a hydrophilic central pore and that this complex can conduct ions. The channel forming hypothesis has been recently questioned by molecular dynamic simulations[15-17]. Molecular dynamic simulations based on new higher resolution NMR structures show that the PLN forms a pore like structure but that this pore is unable to conduct ions[16, 17]. Moreover in a recent paper based on electrochemical measurements it was suggested

that pentamer PLN is just a storage form for monomer and does not generate any channel activity[16]. The authors observed no specific elevation of conductance in a tethered bilayer lipid membrane upon addition of $CaCl_2$ to the buffer solution[16].

In order to understand if PLN pentamer can have ion channel activity, we have performed experiments by using two different biomimetic systems namely supported nanoBLMs and traditional black lipid membranes, BLMs; both systems are characterized by the lipid bilayer membrane(s) separating two compartments (cis and trans) containing aqueous solutions. These experimental systems are suitable for mimicking at the best the intra- and the extra- cellular sides of a biological membrane. The following results, which were obtained by the two complementary approaches show that PLN conducts ions across a lipid bilayer by an inherent ion channel activity.

2 Material and Methods

2.1 nanoBLMs

nanoBLMs consist of polycarbonate membranes (characterized by 1 μm diameter pores, pore density 10^5-10^8 pores$*$cm^{-2} according to pore size, Whatman Kent, England) covered by gold and octadecanethiol. For Au covering a Coating Unit PS3 (Agar Aids, UK) was used. A self-assembled monolayer of octadecanethiol (ODT) (Sigma-Aldrich, USA) was obtained by spreading 3mM ethanolic solution of ODT on the gold layer. Subsequently the ethanol was allowed to evaporate totally and the membrane was rinsed by a series of washing steps in ethanol, water and ethanol to eliminate ODT residues; at the end it was totally dried. On the top of the gold-polycarbonate membrane, an octadecanethiol self assembled monolayer (SAM-ODT) was formed. A lipid bilayer were formed on each pore of the polycarbonate membrane using Dioleoyl-Glycero-Phosphocholine (DOPC) (Avanti polar lipids, Alabaster, AL, USA) and cholesterol (Aldrich Chemical Co. USA), as described in Favero et al.[18, 19]. Experimental measurements were performed in a custom-made cell[18, 19]. The bi-cell, which was fabricated by G. Favero et al.[19], was modified including both

the two reference electrodes and the two Au electrodes in the same working cell. Since conductivity measurements are temperature sensitive (2% increase per one °C) the working cell was placed in a termostated chamber kept at 25°C. Solutions were injected into the chamber by using a peristaltic pump (ECONO PUMP, BIO RAD, USA), modified in order to keep the engine out of the Faraday cage.

Phospholamban (PLN), obtained from Veglia's group, was embedded in the bilayer by fusing vesicles containing PLN at a 3:1:1 mass ratio mixture of DOPC:Cholesterol:PLN.

Electrochemical Impedance Spectroscopy (EIS) measurements were recorded by a PGSTAT12 Autolab potentiostat/galvanostat (Eco Chemie), with an in-built frequency response analysis FRA2 module. The measurements were controlled by a personal computer, using Autolab FRA software. Potentials were measured versus Ag/AgCl electrodes. Impedance spectra were recorded within a frequency range of $5*10^{-3}$ – 10^{6} Hz and at zero offset potential.

Conductivity measurements were carried out by a 712 Conductometer (Metrohm) modified with a Resistance of 47KΩ in parallel to the working cell. The use of the peristaltic pump and the conductometer interfaced with the computer allows to carry out measurements under constant perfusion of the bi-cells.

2.2 Traditional BLMs

Experiments with planar lipid bilayers were carried out as described previously[20] using the Montal-Müller technique[21] with a 0.4 mg/ml solution of L-α-phosphatidylcholine (type IV-S >= 30 % TLC; Sigma-Aldrich (Steinheim, Germany) in n-decan (Carl Roth, Karlsruhe, Germany). The measurements were perfomed in a buffer containing 500mM KCl, 10 mM Mops/Tris pH 7. The Ag/AgCl electrode in the trans compartment was directly connected to the head stage of a current amplifier (EPC 7, List, Darmstadt, Germany). To prevent surface-potential-effects both electrodes were connected with the bath solution via an agar bridge (2% agarose in 2M KCl). Currents were recorded and stored by an analog/digital-converter (LIH 1600, HEKA electronics, Germany) at 4

KHz after low pass filtering at 1 kHz. Data were analyzed by Patchmaster-Software (HEKA electronics) and Igor Pro (WaveMetrics, Oregon, USA). Before adding the phospholamban (PLN) protein to the trans chamber at a final concentration of ca. 0.3µM the bilayer conductance was recorded for approximately 1 hour in order to exclude artefacts from contaminations. Only bilayers without artefacts were used for recostitution of PLN.

3 Results and Discussion

3.1 nanoBLMs

In the nanoBLMs system we first recorded specific resistance and specific capacitance values to verify the integrity of the membrane and incorporation of PLN. Subsequently conductivity measurements were carried out on the same membrane, where PLN was successfully incorporated.

Specific resistance and specific capacitance values were recorded by performing EIS measurements to verify the integrity of the membrane and PLN incorporation. The respective values were obtained by fitting an equivalent circuit to the experimental data (Figure 1); the data obtained with and without PLN show the same order of magnitude for the specific capacitance (1.4 and 1.3 μFcm^{-2} for nanoBLMs before and after PLN incorporation, respectively) and a decrease in the specific resistance by a factor of 10^4 after PLN incorporation (30.4 and $5.4*10^{-3}$ $M\Omega cm^2$ for nanoBLMs before and after PLN incorporation, respectively). The equivalent circuit describes the electrical properties of the bilayer. The fact that approximately the same capacitance value was recorded in the presence and absence of PLN proves the integrity of the membrane; the decrease in resistance associated with PLN suggests a successful incorporation of phospholamban and the presence of ion conducting pores. It is well known that channel formation by peptides or small proteins in biomimetic models causes specific resistance reduction[22, 23].

Conductivity measurements were started with a background electrolyte before different electrolyte solutions (at two different concentration levels) were allowed to flow (2ml/min) through both cell

compartments. As background electrolyte a 10mM TRIS buffer (pH=7.5) solution was used; after a constant conductance value was reached, this buffer was replaced by a solution containing the background electrolyte plus a fixed concentration (10mM and 20mM) of a suitable electrolyte, i.e. KCl, $NaClO_4$ and ChoCl (choline chloride). To check the system's reversibility, after each electrolyte, the background solution was once again perfused into the bicell.

Figure2 reports the conductivity (κ) value vs. time for nanoBLMs embedding PLN in response to different electrolyte solutions. The data show that the conductivity value of nanoBLMs containing PLN increased when different electrolytes were perfused through the chamber. Addition of electrolytes had no impact on the conductivity value in nanoBLMs in the absence of PLN meaning that the increase in conductivity is a property of PLN. The different tested electrolytes were chosen in such a way to make evident the contribution of different ions to the whole conductivity recorded. In particular, the different recorded conductivity between $NaClO_4$ and NaCl (at the same concentration) can be justified simply on the basis of equivalent conductance values of Cl^- and ClO_4^- (equivalent conductance at infinite dilution is 76.3 and 67.3 Scm^2eq^{-1} respectively) since the Na^+ contribution is the same. Useful information about PLN may be obtained by comparing ChoCl and NaCl conductivity values. By considering the equivalent conductance at infinite dilution of NaCl (126.4 Scm^2eq^{-1}) Cl^- contributes for ca. 60% of the total recorded conductivity. Thus, for ChoCl the expected conductance is >60% of that NaCl at the same concentration if also Cho^+ contribute to the signal. Since the conductance of ChoCl is around 60% of that of NaCl, it is evident that Cho^+ does not give an appreciable contribution to the whole recorded conductance signal. These results suggest that PLN is permeable only to relatively small ions as Na^+, Cl^- and ClO_4^- while bigger ions as Cho^+ are unable to pass trough it.

Presented data together with previous ones[2, 10] are consistent with the view that the pentameric PLN can form non-selective ion conducting pores. Based on their model of a bellflower structure, Oxenoid and Chou suggested that many physiologically relevant ions such as Na^+, K^+, Ca^{2+} and Cl^- are small enough to pass through the narrowest part of the pentamer PLN (diameter ≈3.6Å). In

agreement with the latter model the Cho^+ cation (radius 3.3Å[24]) was found not be conducted, because it is larger than the estimated PLN pore [2].

3.2 Traditional BLMs

To further test the channel forming ability of PLN, the same protein was incorporated in traditional BLM for single channel recordings. Figure 3A shows some representative recordings from these experiments revealing typical current fluctuations between a closed and a defined opening state. Figure 3C illustrates a plot of the unitary open channel currents measured under symmetrical conditions (500 mM KCl) as a function of voltage. The I/V relation is linear, reverses at 0 mV and has a slope conductance of 27pS. In many bilayers an additional smaller conductance was found together with the larger 27pS conductance. Figure 3B shows an example for the independent opening/closing of the two distinctly different conductances. In the example trace obtained at 60mV holding voltage the small conductance is opening on top of the large conductance; both conductances close in opposite sequence. The fact that the two conductances are like in the example always additive means that the low conductance is not a sub-conductance level of the larger one. An I/V plot (Figure 3C) of the small unitary channel fluctuations again reveals a linear relation, which reverses at 0mV and has a conductance of 16pS.

To obtain information on the basic functional parameters of the large and small conductance the channel fluctuations were fitted by the QuB algorithm[26]. Good fits could be achieved assuming a simple o-c model. For a reference voltage of +80mV this procedure yields an open probability (P_0) of 0.5 and 0.1 for the large and the small conductance respectively. The mean open dwell times were 680 ms and 560 ms for the large and small conductance respectively. The open probability and the relatively long open channel dwell times look similar to those reported previously for PLN channel activity[10].

Also in previous experiments[10, 25] small unitary channel fluctuations with two different conductances were observed upon reconstituting full length PLN or the c-terminal fragment (amino

acids 26-52) in lipid bilayers. Worth noting is that the present data and the previous recordings were obtained with different bilayer techniques and in different lipids[10, 25]; this stresses the fact that the channel events recorded with PLN are due to the protein and not a bilayer artefact.

4 Conclusions

In conclusion the present results, obtained by two independent electrophysiological methods and previous works[2, 10, 25], support the view that PLN works as an ion channel. Unlike to what was predicted from molecular models[15-17] the present experimental data show that the PLN pentamer can form a pore permeable to small ions; the protein exhibits gating meaning that it fluctuates between an open and a closed state. In this context it is reasonable to assume that the high-resolution NMR structure and the molecular models simply represent the channel in the closed state. The open/closed dwell times of the PLN channel are in the ms range and hence far too long for being detected in simulations. The present data also provide an explanation for the absence of a measurable Ca^{2+} conductance in a previous study. Since PLN generates a non-selective conductance it is not surprising that an elevation of $CaCl_2$ against a 100 fold higher background of KCl was not generating a measurable current; the current was probably masked by the large KCl conductance.

The demonstration of channel function of PLN is of importance as it can be involved in the regulation of cardiac contraction-relaxation; PLN generated channels could be a promising therapeutic target in heart failure and other cardiac diseases[27, 28]. The integration of both the present experimental systems provides a strong tool for in depth studies of PLN channel function with respect to selectivity and pharmacology.

Acknoledgments

We thank Prof. G.Veglia for providing phospholamban used in this work. The financial support from Ente Cassa di Risparmio di Firenze and Ministero dell'Istruzione, Università e Ricerca (PRIN project), is gratefully acknowledged.

Figure1: Logarithm of the impedance, Z (square symbol) and phase, ϕ (circle symbol) vs. logarithm of the frequency (f): curves recorded on nanoBLMs (filled symbol) and nanoBLMs containing PLN (empty symbol). All data were obtained at zero offset potential. 10mM TRIS buffer pH=7,5 was present into working cell compartments. Inset: Equivalent circuit (C_1= bilayer capacitance; R_2= bilayer resistance; R_1=electrolyte resistance) used to fit the experimental data obtained from the Electrochemical Impedance Spectroscopy.

Figure 2: Conductivity (measured by conductometer) vs. time, recorded on PLN embedded in nanoBLMs. Data were collected under constant perfusion (2 ml/min) of bicells. Experiment started with only TRIS buffer 10mM, pH=7,5 [C(0)] in the bicell. The solution was exchanged by flowing into bicell compartments TRIS plus one of the following electrolyte: ChoCl, $NaClO_4$ and NaCl at different concentration [C(1)=ChoCl 10mM, C(2)=ChoCl 20mM, C(3)= $NaClO_4$ 10mM, C(4)= $NaClO_4$ 20mM C(5)= NaCl 10mM, C(6)= NaCl 20mM] in TRIS-HCl buffer 10mM, pH=7,5.

Figure 3: PLN generates single channel fluctuations in planar lipid bilayer. (A) Single channel activity recorded at different holding potentials, from -120mV to 120mV in symmetrical solution with 500mM KCl in 10mM MOPS/TRIS (pH=7) buffer. c and o refer to the closed and open states of the channel, respectively. (B) Example of concomitant opening/closing of large conductance and small conductance. The two events are additive. First the large conductance opens (o_l) before also a lower conductance opens (o_s). Together the current reaches the sum of both amplitudes (o_l+o_s). Upon closing of the large conductance the current reaches the amplitude of the small conductance. Closing of the small conductance brings the current back to the baseline (c). (C) Current/voltage relation of large and small unitary currents obtained in same conditions as in A and B.

[1] R. L. Cornea, L. R. Jones, J. M. Autry, and D. D. Thomas, Mutation and Phosphorylation Change the Oligomeric Structure of Phospholamban in Lipid Bilayers, Biochemistry. 36 (1997) 2960-2967.

[2] K. Oxenoid, and J. Chou, The structure of phospholamban pentamer reveals a channel-like architecture in membranes., Proc. Natl. Acad. Sci. U S A. 102 (2005) 10870-10875.

[3] J. Zamoon, A. Mascioni, D. D. Thomas, and G. Veglia, NMR Solution Structure and Topological Orientation of Monomeric Phospholamban in Dodecylphosphocholine Micelles, Biophys. J. 85 (2003) 2589-2598.

[4] Y. Kimura, K. Kurzydlowski, M. Tada, and D. H. MacLennan, Phospholamban Inhibitory Function Is Activated by Depolymerization, J. Biol. Chem. 272 (1997) 15061-15064.

[5] L. G. Reddy, L. R. Jones, and D. D. Thomas, Depolymerization of Phospholamban in the Presence of Calcium Pump: A Fluorescence Energy Transfer Study., Biochemistry 38 (1999) 3954-3962.

[6] D. L. Stokes, A. J. Pomfret, W. J. Rice, J. P. Glaves, and H. S. Young, Interactions between Ca^{2+}-ATPase and the Pentameric Form of Phospholamban in Two-Dimensional Co-Crystals, Biophys. J. 90 (2006) 4213-4223.

[7] N. J. Traaseth, R. Verardi, K. D. Torgersen, C. B. Karim, D. D. Thomas, and G. Veglia, Spectroscopic validation of the pentameric structure of phospholamban, Proc. Natl. Acad. Sci. U S A. 104 (2007) 14676-14681.

[8] S. Tatulian, L. Jones, L. Reddy, D. Stokes, and L. Tamm, Secondary structure and orientation of phospholamban reconstituted in supported bilayers from polarized attenuated total reflection FTIR spectroscopy., Biochemistry 34 (1995) 4448-4456.

[9] I. T. Arkin, M. Rothman, C. F. C. Ludlam, S. Aimoto, D. M. Engelman, K. J. Rothschild, and S. O. Smith, Structural Model of the Phospholamban Ion Channel Complex in Phospholipid Membranes, J. Mol. Biol. 248 (1995) 824-834.

[10] R. Kovacs, M. Nelson, H. Simmerman, and L. Jones, Phospholamban forms Ca^{2+}-selective channels in lipid bilayers, J. Biol. Chem. 263 (1988) 18364-18368.

[11] H. K. B. Simmerman, Y. M. Kobayashi, J. M. Autry, and L. R. Jones, A Leucine Zipper Stabilizes the Pentameric Membrane Domain of Phospholamban and Forms a Coiled-coil Pore Structure, J. Biol. Chem. 271 (1996) 5941-5946.

[12] I. Arkin, P. Adams, K. MacKenzie, M. Lemmon, A. Brünger, and D. Engelman, Structural organization of the pentameric transmembrane alpha-helices of phospholamban, a cardiac ion channel., EMBO J. 13 (1994) 4757–4764.

[13] I. Arkin, P. Adams, A. Brünger, S. Smith, and D. Engelman, Structural perspectives of phospholamban, a helical transmembrane pentamer., Annu. Rev. Biophys. Biomol. Struct. 26 (1997) 157-179.

[14] M. Sansom, G. Smith, O. Smart, and S. Smith, Channels formed by the transmembrane helix of phospholamban: a simulation study., Biophys. Chem. 69 (1997) 269-281.

[15] T. Kim, J. Lee, and W. Im, Molecular dynamics studies on structure and dynamics of phospholamban monomer and pentamer in membranes, Proteins. 76 (2009) 86-98.

[16] L. Becucci, A. Cembran, C. B. Karim, D. D. Thomas, R. Guidelli, J. Gao, and G. Veglia, On the Function of Pentameric Phospholamban: Ion Channel or Storage Form?, Biophysical J. 96 (2009) L60-L62.

[17] C. Maffeo, and A. Aksimentiev, Structure, Dynamics, and Ion Conductance of the Phospholamban Pentamer, Biophysical J. 96 (2009) 4853-4865.

[18] G. Favero, A. D'Annibale, L. Vampanella, R. Santucci, and T. Ferri, Membrane supported bilayer lipid membranes array: preparation, stability and ion-channel insertion, Anal. Chim. Acta. 460 (2002) 23-34.

[19] G. Favero, L. Campanella, A. D'Annibale, R. Santucci, and T. Ferri, Mixed hybrid bilayer lipid membrane incorporating valinomycin: improvements in preparation and functioning, Microchem. J 74 (2003) 141-148.

[20] H. Schrempf, O. Schmidt, R. Kümmerlen, and R. Wagner, A prokaryotic potassium ion channel with two predicted transmembrane segments from Streptomyces lividans., EMBO J. 14 (1995) 5170–5178.

[21] M. Montal, and P. Mueller, Formation of Bimolecular Membranes from Lipid Monolayers and a Study of Their Electrical Properties, Proc. Natl. Acad. Sci. U S A. 69 (1972) 3561-3566.

[22] E. Gallucci, S. Micelli, and V. Picciarelli, Multi-channel and single-channel investigation of protein and peptide incorporation into BLM, in Planar Lipid Bilayer (BLMs) and their applications, in Tien, H. T., and Ottova-Leitmannova, A., (Eds.), Elsevier, Amsterdam, 2003, pp. 413 - 447.

[23] S. Terrettaz, M. Mayer, and H. Vogel, Highly Electrically Insulating Tethered Lipid Bilayers for Probing the Function of Ion Channel Proteins, Langmuir 19 (2003) 5567-5569.

[24] D. G. Levitt, and E. R. Decker, Electrostatic radius of the gramicidin channel determined from voltage dependence of H+ ion conductance., Biophys. J. 53 (1988) 33-38.

[25] I. T. Arkin, in, 1995 University of Yale.

[26] F. Qin, and L. Li, Model-Based Fitting of Single-Channel Dwell-Time Distributions, Biophysical J. 87 (2004) 1657-1671.

[27] A. G. Brittsan, and E. G. Kranias, Phospholamban and Cardiac Contractile Function, J. Mol. Cell. Cardiol. 32 (2000) 2131-2139.

[28] D. H. MacLennan, and E. G. Kranias, Phospholamban: a crucial regulator of cardiac contractility, Nat. Rev. Mol. Cell. Biol. 4 (2003) 566-577.

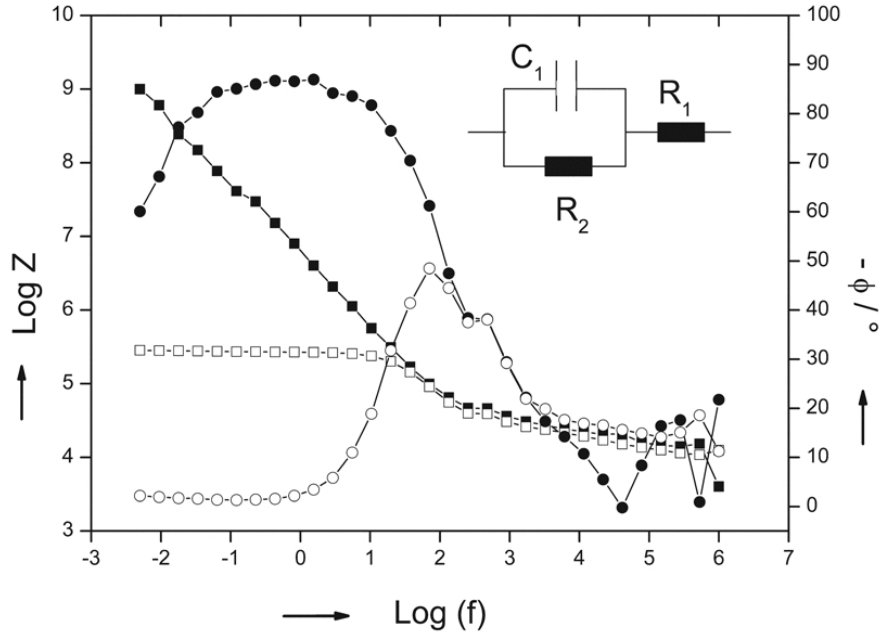

Figure 1

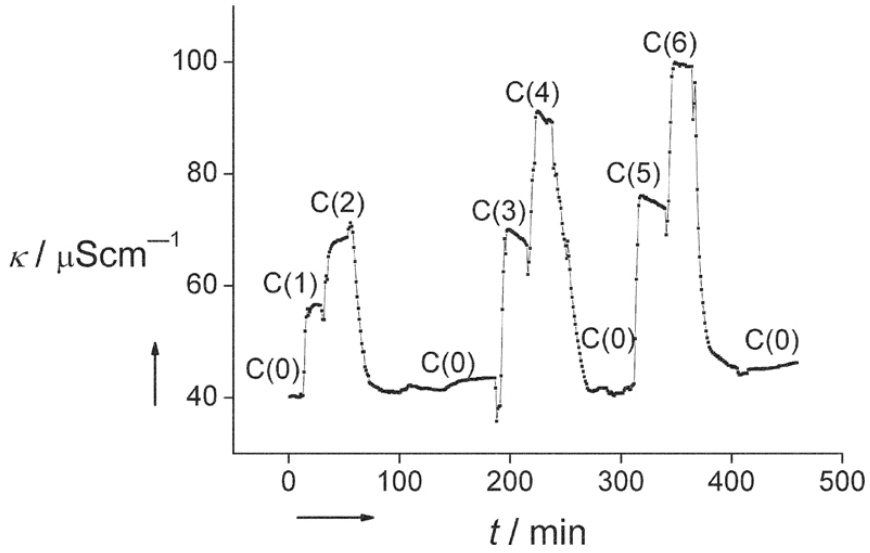

Figure 2

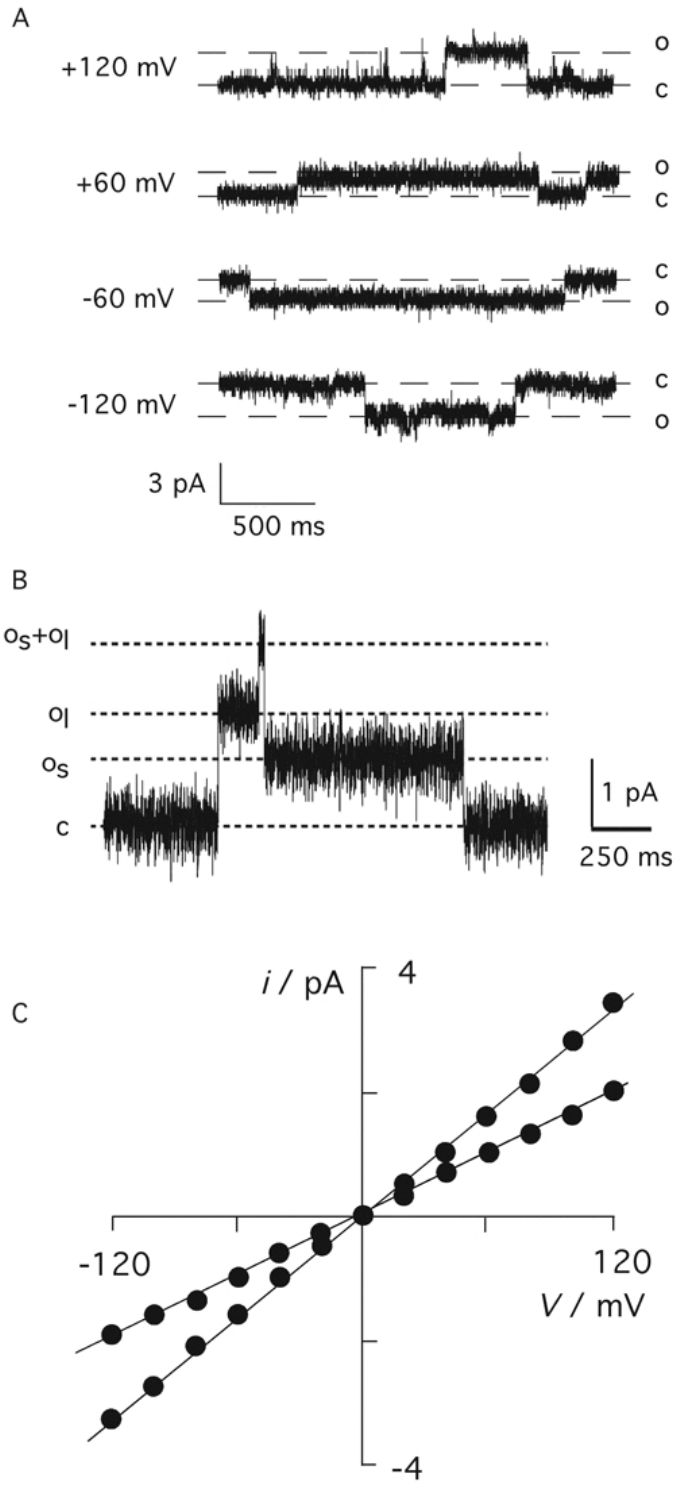
A
+120 mV
+60 mV
-60 mV
-120 mV
o
c
3 pA
500 ms
B
o_S+o_I
o_I
o_S
c
1 pA
250 ms
C
i / pA
4
-4
-120
120
V / mV

Figure 3

Bibliography

[1] Lipowsky, R.; Sackmann, E. *Structure and Dynamics of Membranes*; Elsevier Science, 1995; Vol. 1A.

[2] Tien, H.; Ottova-Leitmannova, A. *Membrane Biophysics as viewed from experimental bilayer lipid membrane*; Elsevier Science, 2000.

[3] Favero, G.; D'Annibale, A.; Campanella, L.; Santucci, R.; Ferri, T. *Anal. Chim. Acta.* **2002**, *4*, 23–34.

[4] Vallejo, A.; Gervasi, C. *Bioelectrochemistry* **2002**, *57*, 1–7.

[5] Chugh, J.; Wallace, B. *Biochem. Soc. Trans.* **2001**, *29*, 565–70.

[6] Brogden, K. *Nat. Rev. Microbiol.* **2005**, *3*, 238–50.

[7] Schmidt, A.; Edes, I.; Kranias, E. *Cardiovasc Drugs Ther.* **2001**, *15*, 387–96.

[8] Cornea, R. L.; Jones, L. R.; Autry, J. M.; Thomas, D. D. *Biochemistry.* **1997**, *36*, 2960–2967, TY - JOUR doi: 10.1021/bi961955q DO - 10.1021/bi961955q.

[9] Oxenoid, K.; Chou, J. *Proc. Natl. Acad. Sci. U S A.* **2005**, *102*, 10870–5.

[10] Zamoon, J.; Mascioni, A.; Thomas, D. D.; Veglia, G. *Biophys. J.* **2003**, *85*, 2589–2598.

[11] Kimura, Y.; Kurzydlowski, K.; Tada, M.; MacLennan, D. H. *J. Biol. Chem.* **1997**, *272*, 15061–15064.

[12] Reddy, L. G.; Jones, L. R.; Thomas, D. D. *Biochemistry.* **1999**, *38*, 3954–3962.

[13] Stokes, D. L.; Pomfret, A. J.; Rice, W. J.; Glaves, J. P.; Young, H. S. *Biophys. J.* **2006**, *90*, 4213–4223.

[14] Traaseth, N.; Verardi, R.; Torgersen, K.; Karim, C.; Thomas, D.; Veglia, G. *Proc. Natl. Acad. Sci. U S A.* **2007**, *104*, 14676–81.

[15] Tatulian, S.; Jones, L.; Reddy, L.; Stokes, D.; Tamm, L. *Biochemistry.* **1995**, *34*, 4448–56.

[16] Arkin, I. T.; Rothman, M.; Ludlam, C. F.; Aimoto, S.; Engelman, D. M.; Rothschild, K. J.; Smith, S. O. *J. Mol. Biol.* **1995**, *248*, 824–834.

[17] Brittsan, A.; Kranias, E. *J Mol Cell Cardiol.* **2000**, *32*, 2131–9.

[18] MacLennan, D.; Kranias, E. *Nat. Rev. Mol. Cell. Biol.* **2003**, *4*, 566–77.

[19] Dodelet-Devillers, A.; Cayrol, R.; van Horssen, J.; Haqqani, A.; de Vries, H.; Engelhardt, B.; Greenwood, J.; Prat, A. *J. Mol. Med.* **2009**, *87*, 765–74.

[20] Simons, K.; Ehehalt, R. *J. Clin. Invest.* **2002**, *110*, 597–603.

[21] Muller, P.; Rudin, D.; Tien, H.; Wescott, W. *Nature* **1962**, *194*, 979–980.

[22] Montal, M.; Mueller, P. *Proc. Natl. Acad. Sci. U S A.* **1972**, *69*, 3561–6.

[23] Coronado, R.; Latorre, R. *Biophys. J.* **1983**, *43*, 231–6.

[24] Tien, H.; Ottova, A. *Colloids Surf. A Physicochem. Eng. Asp.* **1999**, *149*, 217–233.

[25] Favero, G.; Campanella, L.; Cavallo, S.; D'Annibale, A.; Perrella, M.; Mattei, E.; Ferri, T. *J. Am. Chem. Soc.* **2005**, *127*, 8103–11.

[26] Strobel, H.; Heineman, S. *Chemical Instrumentation: A systematic approach. Third edition*; Wiley Interscience, 1989.

[27] Gallucci, E.; Micelli, S.; Picciarelli, V. In *Planar Lipid Bilayer (BLMs) and their applications*; Tien, H., Ottova-Leitmannova, A., Eds.; Elsevier, 2003; Chapter Multi-channel and single-channel investigation of protein and peptide incorporation into BLM, pp 413 – 447.

[28] Terrettaz, S.; Mayer, M.; Vogel, H. *Langmuir* **2003**, *19*, 5567–5569.

[29] Gualdani, R. M.Sc. thesis, University of Florence, 2006.

[30] Kovacs, R.; Nelson, M.; Simmerman, H.; Jones, L. *J. Biol. Chem.* **1988**, *263*, 18364–18368.

[31] Levitt, D. G.; Decker, E. R. *Biophys. J.* **1988**, *53*, 33–38.

[32] Qin, F.; Li, L. *Biophysical J.* **2004**, *87*, 1657–1671.

[33] Arkin, I. T. Ph.D. thesis, University of Yale, 1995.

[34] Baldini, C.; Peggion, C.; Falletta, E.; Moncelli, R., M.R. amd Guidelli; Toniolo, C. A Lipid Monolayer Made Permeable to Tl(I) Ions by the Lipopeptaibol Trichogin GA IV. *Understanding Biology Using Peptides*, 2006; pp 265–266.

[35] Mazzuca, C.; Stella, L.; Venanzi, M.; Formaggio, F.; Toniolo, C.; Pispisa, B. *Biophys J.* **2005**, *88*, 3411–21.

[36] Bocchinfuso, G.; Palleschi, A.; Orioni, B.; Grande, G.; Formaggio, F.; Toniolo, C.; Park, Y.; Hahm, K.; Stella, L. *J. Pept. Sci.* **2009**, *15*, 550–8.